Stability analysis of microwave circuits

Almudena Suárez

Dpto. Ingeniería de Comunicaciones

University of Cantabria, Spain

Introduction

Instability problems often faced by designers of nonlinear microwave circuits are the cause of significant qualitative discrepancies between simulations and measurements, even when using powerful simulation tools, based on harmonic-balance analysis and numerical optimization algorithms. Critical anomalies resulting from these instability phenomena most often invalidate the prototype and demand intense investigation and resolution efforts, which may substantially increase the production cycles and final cost. Understanding instability requires awareness of the two facts: two or more steady-state solutions can coexist for the same values of the circuit elements and stable solutions must be able to recover against the small perturbations that are always present in real life. To realize the complexity of the problem, one must take into account that circuits containing nonlinear components, such as transistors and diodes, are governed by a set of nonlinear differential algebraic equations [1-4]. Time differentiation comes from the existence of reactive elements, involving this operation in their constitutive relationships, and nonlinearity comes from the presence of semiconductor devices, containing nonlinear functions in their intrinsic models. Nonlinear differential equation systems admit four main types of steady-state solutions: *dc*, periodic, quasi-periodic (having two or more fundamental frequencies with non-rational relationships) or chaotic (non-periodic) [1,5-7]. Unexpected solutions are often observed in nonlinear circuits, since, in addition to the frequencies delivered by the input sources, there may be frequency components coming from the circuit self-oscillation. For instance, under a periodic excitation at ω_{in}, the solution measured may not be periodic at ω_{in}. Instead, it may be quasiperiodic at ω_{in} and an oscillation frequency ω_o, it may exhibit a subharmonic oscillation at $\omega_{in}/2$ or exhibit a continuous spectrum (chaos) [7-8].

Frequency-domain analysis methods, such as scattering parameters or harmonic balance, are applied under the constraint of a particular waveform. For instance, in the S parameter analysis of an amplifier, the small-signal solution is assumed to be sinusoidal at the frequency of the input source [9], and in the harmonic balance analysis of a power amplifier, the solution is assumed to be periodic at the frequency of the driving source, with a certain harmonic content [4,10-11]. This particularization prevents obtaining other possible and more complex circuit solutions. One essential fact is that two or more steady-state solutions (of the same or different type) may coexist for the same values of the circuit elements and parameters. All the coexisting solutions will be mathematically valid. However, only *stable* solutions can be physically observed, since only stable solutions are robust against the small perturbations that are always present in real life, coming from noise and perturbations. When a stable solution undergoes a small instantaneous perturbation, the transient response is such that the system returns to this solution exponentially in time. In contrast, the small perturbation of an unstable solution makes the system evolve to a qualitatively different (and stable) steady-state solution. Therefore, if the solution simulated is unstable, it will not be observed experimentally.

When particularizing the analysis to a given type of waveform, as done with scattering parameters or with harmonic balance, the solution obtained will be mathematically valid, but it might not be stable (or physical) [7-8]. The only way to verify the physical existence of a given steady state solution is to perform a stability analysis [12-13]. The problem generally relies on the existence of a self-oscillation, which is not detected by the simulation method. As an example, Fig. 1(a) and Fig. 1(b) compare the solution simulated with harmonic balance and the solution measured for the same values of the circuit elements and parameters. The solution simulated is periodic, whereas the solution measured corresponds to a quasi-periodic regime with two fundamental frequencies: the input frequency ω_{in} and a self-generated oscillation. The periodic solution is unstable and this is why it cannot be measured. In contrast, the coexisting quasi-periodic solution is stable and this is why it is obtained experimentally.

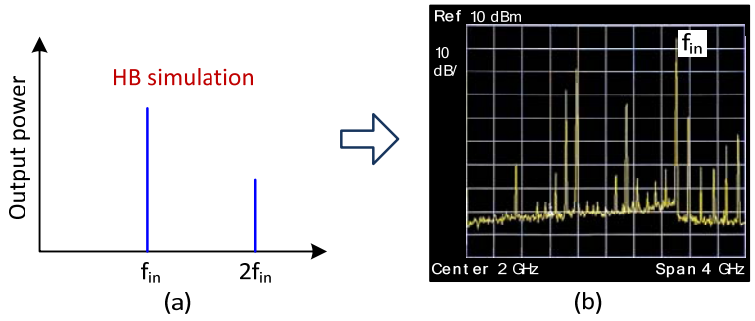

Fig. 1 Coexistence of steady-state solutions. (a) Solution simulated with harmonic balance. It is mathematically valid but unstable (unphysical). (b) Measured solution for the same values of the circuit elements and parameters. It is stable or *robust*.

The instability mechanism leading to an ordinary oscillation can be understood as the effect a closed loop composed of a gain stage and positive feedback [12], such that the gain exceeds the feedback loss at a particular frequency. Alternatively, it can be understood as due to an excess of negative resistance at a resonant frequency [14]. Indeed, current passing through a negative resistance delivers energy to the circuit, unlike the case of a positive resistance, which implies energy consumption. The energy excess at a resonant frequency leads to the growth of a transient oscillation at the resonance frequency. The active elements are nonlinear and from certain amplitude, negative resistance must physically decrease, which allows reaching the steady-state oscillation for a perfect balance of power delivered and consumed. To make things more complex, circuits that are stable in small signal may become unstable under a large-signal drive at ω_{in} [15-17]. This can be due to gain expansion, especially in the case of devices biased below conduction threshold, or to negative resistance exhibited by the nonlinear capacitances existing in transistors and diodes under large-signal periodic pumping [18-19]. The energy delivered by the pump signal gives rise to negative resistance around the original resonance frequency of the capacitor with an inductive element, in small signal conditions. A *parametric* oscillation [18-19] will arise if, from certain input power, the negative resistance dominates the loss effects, which will most likely occur if the frequency of the pump signal is about twice the frequency of the original resonance frequency. The described oscillation will enable the

implementation of parametric frequency dividers, but will be undesired in parametric amplifiers [9] and diode-based multipliers [19].

Examples of instability phenomena

Instability is extremely common in nonlinear circuits. As just mentioned, it can be the mechanism to obtain the desired operation regime or it can be unwanted. Examples of circuits requiring instability phenomena are oscillators and frequency dividers [20]. In each case, the desired steady-state regime (free-running oscillation or frequency division) coexists with another steady-state solution, which should be unstable for a regular behavior [1-2]. On the one hand, any free-running oscillator circuit can be resolved for a *dc* solution, due to the absence of any time-varying input sources. This solution has to be unstable (at about the desired oscillation frequency) to enable the oscillation start-up from the noise level. However, the desired periodic steady-state oscillation must be stable, or able to recover under small perturbations. On the other hand, any frequency divider circuit [20] can be resolved for a non-divided solution at the frequency of the input drive ω_{in}, acting as a sole independent periodic source. This solution must be unstable at the subharmonic frequency to enable the build-up of the divided regime. In contrast, the desired divided solution must be stable or *robust*.

However, in many cases instability is unwanted, like in low noise amplifiers, frequency mixers [21], power amplifiers or frequency multipliers [19], for instance, which do not require oscillations of any kind. Some examples are cited in the following. Instability of the *dc* regime (in a small-signal amplifier, for instance) may lead to an oscillation in the absence of input sources, with a behavior similar to that of a free-running oscillator. On the other hand, a circuit, expected to operate in large-signal regime, such as a power amplifier, may be stable in the absence of input drive, with instability arising from certain power level at the input frequency ω_{in} [8,16-17]. The large-signal periodic regime becomes unstable at this power level and this instability may lead to a quasi-periodic solution (two non-rationally related fundamental frequencies) at ω_{in} and ω_o [as in Fig. 1(b)] or to a frequency division by 2. As an example, the

measurements of Fig. 2, corresponding to a power amplifier, show a frequency division by 2 when increasing the input power. The spectra in Fig. 2(a) and Fig. 2(b) present the solutions measured for two different values of input power, P_{in1} and P_{in2}. For P_{in1}, the periodic solution at the input frequency ω_{in} is stable and the spectrum measured at this fundamental frequency is shown in Fig. 2(a). For the larger input power P_{in2}, this periodic solution is unstable, and the measured spectrum corresponds to a different solution: a divided-by-two regime [Fig. 2(b)]. In consistency with the reasoning above, for P_{in2}, a non-divided mathematical solution at ω_{in} coexists with the divided regime as an unstable mathematical solution. This is similar to the coexistent unstable and stable solutions shown in Fig. 1(a) and Fig. 1(b).

Transitions to a quasi-periodic regime at ω_{in} and ω_o [Fig. 1(b)] or to a suharmonic regime at $\omega_{in}/2$ [Fig. 2(b)] are fundamental instability phenomena which may be followed by other effects that would make the solution even more complex. For instance, after observation of a quasi-periodic solution at ω_{in} and ω_o, there can be a sub-synchronization of the oscillation to the input frequency [17], giving rise to frequency division by an order n in a certain parameter interval. Another possibility is the onset of a second oscillation frequency ω_o', which will likely lead the circuit into a chaotic regime, characterized by a sensitivity dependence on the initial conditions and the nonperiodicity of the solution waveform [8]. Note, however, that there are other instability mechanisms leading to chaotic regime, known as *routes to chaos* [22-23].

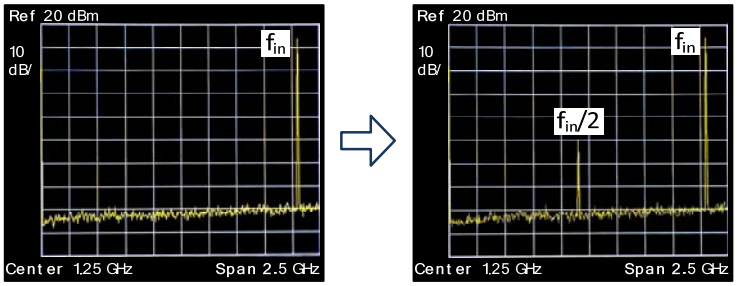

Fig. 2 Frequency division two when increasing the input power. (a) Measured periodic solution for the input power P_{in1}. (b) Measured subharmonic solution for the higher input power P_{in2}.

Another major form of unwanted behavior is hysteresis or jumps observed when varying a circuit parameter [17]. See an example in Fig. 3. It is the power transfer curve of a power amplifier [24]. For input power (P_{in}) between T_1 and T_2, the amplifier has three valid mathematical solutions. Solutions in the middle section (s_2) are unstable. However, solutions in the lower section (s_1) and in the upper section (s_3) are stable and can be measured experimentally. Each coexisting stable solution has its own *basin of attraction* or set of initial values such that the system evolves to the particular steady-state solution. These initial values are conditioned by the sense of variation of P_{in}. Thus a hysteresis phenomenon [5,24] is observed when increasing and decreasing P_{in}.

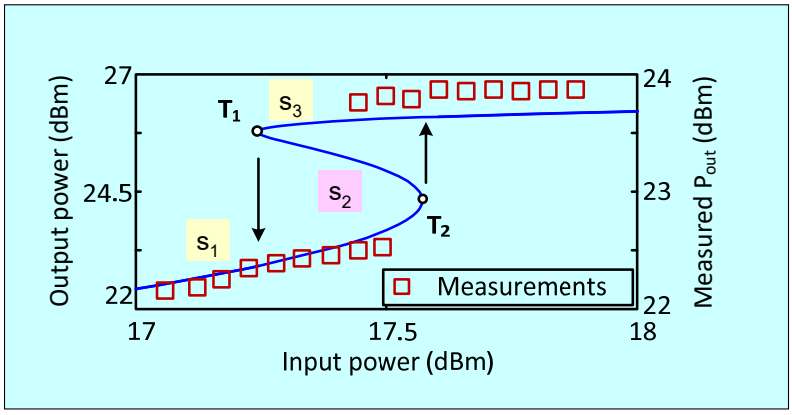

Fig. 3 Hysteresis cycle in the power transfer curve of a power amplifier [24]. In the input power interval comprised between T_1 and T_2 there is a coexistence of three solutions, of the types S_1, S_2 and S_3. Solutions of the type S_1 and S_3 are stable. Solutions of the type S_2 are unstable.

Need for a complementary stability analysis

Even though the mechanisms leading to the major forms of instability are generally well understood, an *a priori* prediction of unstable behavior in a practical microwave circuit with full models of its active and passive elements is usually impossible, unless a rigorous stability analysis is carried out. To understand the problem, one must take into account that the number of resonance frequencies increases with the number of reactive elements, and the potential number of unstable loops increases with the number of active devices [16,25-26]. Regarding the

possible instability of the *dc* solution, circuits based on devices exhibiting broadband gain must be examined carefully as there can be resonance frequencies within the whole band [21], susceptible to give rise to instability, including low-frequency resonances associated to the bias networks. On the other hand, to avoid large-signal instability due to gain expansion, one should ensure small-signal stability for all the device bias conditions comprised in the large-signal excursion of the device voltages or currents [24]. The parametric oscillations, due to nonlinear capacitances, are more difficult to anticipate. However, these will arise more likely if the input frequency is near twice the resonance frequency of a nonlinear capacitance and this resonance has a low damping effect [2,18].

Taking into account the high number of passive and/or active elements in most practical nonlinear circuits, the fact that the circuit can be unstable in small signal and/or large signal and the variety of instability phenomena, one can conclude that the only way to accurately predict undesired instability phenomena is to complement the frequency-domain simulation with a rigorous stability analysis. The difficulties of the widely used harmonic-balance method for the analysis/prediction of self-oscillations [5-7,20] are briefly explained in the following. Harmonic balance only provides steady-state solutions, represented with a Fourier series, usually in terms of one or two fundamental frequencies. The harmonic balance system is constituted by a set of nonlinear algebraic equations, which are solved through an error-minimization technique [4,10-11], usually the Newton-Raphson algorithm. This algorithm is sensitive to the initial value, which will lead to trouble in the case of coexistence of steady-state solutions.

As already stated, solutions containing either non-harmonic or subharmonic oscillations, always coexist with solutions at the frequencies delivered by the input sources, for which the circuit does not oscillate, such as the *dc* solution of a free-running oscillator. Because the harmonic-balance method only provides steady-state solutions, it is insensitive to the stability properties of these solutions, which would require the capability to predict their transient reaction to small perturbations. If two or more solutions coexist, default convergence of the error-minimization method will lead to the least demanding solution. In a free-running oscillator, default convergence would lead to the *dc* solution, this is why *Oscports* [11] or other

complementary procedures [5,20] must be used for oscillator analysis. To obtain an oscillatory solution, two conditions must be fulfilled: the fundamental oscillation frequency ω_o should be considered in the Fourier series representation of the circuit variables and the harmonic-balance system must be suitably initialized. In comparison, the time domain analysis transforms the continuous-time nonlinear differential-equation system into a discrete time system [1,4]. This involves replacing the time differentiation by a particular algebraic expression of the time derivatives in terms of the present sample and previous time samples (*implicit methods*). The resulting nonlinear algebraic equation is resolved at each time point t_n and the waveform is obtained by assembling all the sequence of solutions (t_n, x_n). Provided the integration method (expression of the time derivative) and time step are properly selected [1], the time evolution of the circuit variables will emulate the physical evolution of these variables from the initial condition to the steady-state regime.

To summarize, the frequency domain analysis only provides steady state solutions of particular type and are insensitive to the stability properties of the solution obtained. To check the physical observability of the solutions, the frequency domain analysis must be extended so as to consider the effect of small perturbations on the steady-state solution. One should emphasize that the perturbations considered must be of small amplitude. This is because in a nonlinear differential-equation system two or more stable solutions may coexist, each one being to recover under small perturbations coming from noise, etc, and thus being stable or robust. This can be understood from inspection of Fig. 3. Let a P_{in} value comprised between T_1 and T_2 be assumed. When applying a large perturbation the system may evolve from either the upper stable solution (s_3) to the lower stable solution (s_1) or vice versa. A large perturbation may lead the system from one stable solution to another and our conclusion on the robustness of the solution would be wrong. Therefore, one must keep in mind that the stability properties are inherently local and the stability test must always be performed under small perturbations.

In this article, the most relevant stability analysis method will be introduced from a historical perspective. For a detailed comparison of their foundations, ease of implementation and capabilities, they will be applied to simple circuits, which will enable a thorough analytical

evaluation and comprehension. Such level of detail would be impossible with practical examples due to their high order, given, in lumped circuits, by the number of reactive elements. The methods considered are the Rollet stability analysis [9,27], applicable to *dc* solutions only, the Nyquist stability analysis of the characteristic system [15,16], the normalized determinant function [16,25-26] and pole-zero identification [28-31]. The three last methods are accurate and complete and can be applied to both dc and periodic solutions. However, thee three methods have different conditionings and properties that will be shown through the article and are briefly summarized in Table I.

Rollet's stability analysis

Rollet's stability analysis was published in 1962 [27]. This analysis is intended for two-port networks expected to operate in linear regime with respect to an input source at the frequency ω_{in}. The aim is to prevent the possible self-oscillation of the network under certain loading conditions of the two-port. Instability may lead to a qualitatively different *dc* operation point, but in most cases it will lead to a large signal oscillation at a frequency ω_o at the expense of the energy delivered by dc sources. Obviously, because the circuit behaves linearly with respect to the input source at ω_{in}, superposition applies and the circuit stability can be analyzed suppressing this input source. Remind that in measurements the so-called small signal instabilities are observed by simply biasing the active components, prior to the connection of the RF input sources, since they do not come from these sources. They are due to the instability of the *dc* regime.

The aim of the Rollet stability criteria is to prevent the two-port network [containing the active device(s)] from exhibiting negative resistance when looking into its input or output, in order to avoid the energy unbalance that would lead to a possible instability of the *dc* solution. Assuming that the two-port network fulfills the so-called *Rollet proviso* [27,32-34], to be discussed later, the two-port network will be absolutely stable if it does not exhibit negative resistance at its input (output) for any passive load (source) impedance, connected to the opposite port. The absolute stability conditions are written in a compact manner in terms of the

Rollet factor k and the determinant of the scattering matrix (or alternatively, the μ factor [34]). If the two-port network is not absolutely stable, input and output passive loads should be restricted to certain regions of the Smith chart, delimited by the stability circles [9].

Table I Brief comparison between the main stability analysis methods.

Method	**Applicable to commercial HB?**	**Dependent on observation port?**	**Relevant characteristics**
Analysis of characteristic system	No. It requires access to Jacobian matrix of nonlinear functions.	No	It would be definitive if one could calculate the complex roots of the characteristic determinant. Nyquist analysis is applied to determine number of unstable roots.
Normalized-determinant function	Yes	No	It is based on an open-loop analysis that requires access to the device intrinsic nonlinear models. To open the model, the device control voltage is replaced with an independent excitation signal.
Pole-zero identification	Yes	It may depend, due to possible pole-zero cancellations	It is a closed-loop method that does not require access to the device models. It is easy to apply through simple introduction of an independent small signal source at a sensitive location. It provides not only the number of unstable poles but also the values of these poles. The pole evolution under variation of a parameter can be obtained through a sequence of two-stage analyses: steady-state calculation, plus pole-zero identification.

The perturbation frequency considered in the analysis must vary from *dc* to the highest frequency at which the active devices may exhibit gain. Note that the physical perturbations coming from noise will expand through the whole spectrum, obviously including the circuit

critical-resonance frequencies. When using the so called stable loads (within the stable regions of the source and load Smith charts), the two-port network will exhibit input and output impedances with positive real part. However, this will only imply absolute stability if the Rollet *proviso* is fulfilled. The proviso takes into account the limited observability of the two-port network from its input and output ports. Indeed, the network may contain instability mechanisms that are not observable from the input and output. As can be easily understood, this lack of observability is more likely in circuits with complex topologies, although there are simple counter-examples too [32]. In order for the input/output observation to be sufficient, the two-port network must fulfill the *Rollet proviso* [32-33], which ensures that the two-port is stable on its own, that is, when loaded with infinite and zero impedances. If the two-port network is unstable in these conditions, the instability might remain when the circuit is loaded with passive impedances, even when though this instability is not detected from the analysis of the input and output impedances of the two-port network.

Two examples are shown in Fig. 4. The circuit in Fig. 4(a) is unstable when terminated in open circuits and the one in Fig. 4(b) is unstable when terminated in short circuits. Let us consider first the circuit in Fig. 4(a), with termination ports used to measure the scattering parameters. For $R_1 \| R_2 > -1/G_3$, the input and output impedances of the two-port network will always have a positive real part, corresponding to stable behavior with the ill-applied Rollet criterion. As shown in the analysis of Fig. 5(a), it exhibits $\mu > 1$ for all the perturbation frequencies. However, when connecting any passive resistances R_1 and R_2, such that $R_1 \| R_2 > -1/G_3$, the circuit will oscillate [Fig. 5(b)]. This is because the small value of negative resistance in parallel dominates the positive one. For the circuit in Fig. 4(b), the situation is the dual one. When connecting any passive resistances R_1 and R_2, such that $R_1 + R_2 < -R_3$, the circuit will oscillate [Fig. 5(d)]. However, it fulfills $\mu > 1$ for all the perturbation frequencies [Fig. 5(c)]. The apparent contradiction is due to the fact that when defining the two-port network for the evaluation of μ we "break" the circuit at the defined reference planes. We change the nature of the series (Fig. 4a) or parallel (Fig. 4b) connection of

the active element to its passive loads, so the unstable resonance is dominated in each case by other impedance contributions.

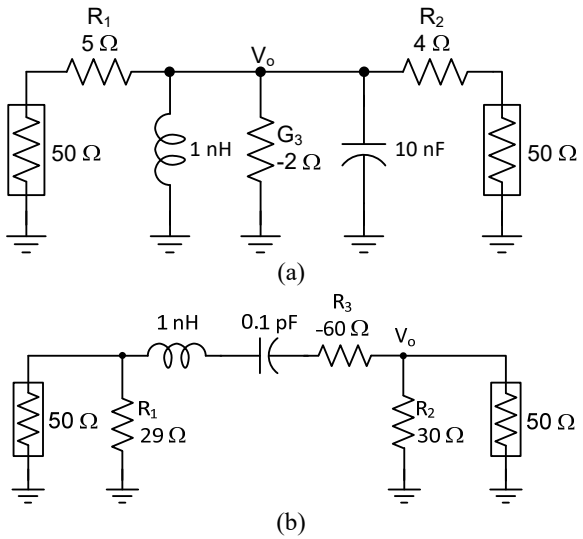

Fig. 4 Two simple circuits that do not fulfill the *Rollet proviso*. (a) Parallel configuration. (b) Series configuration.

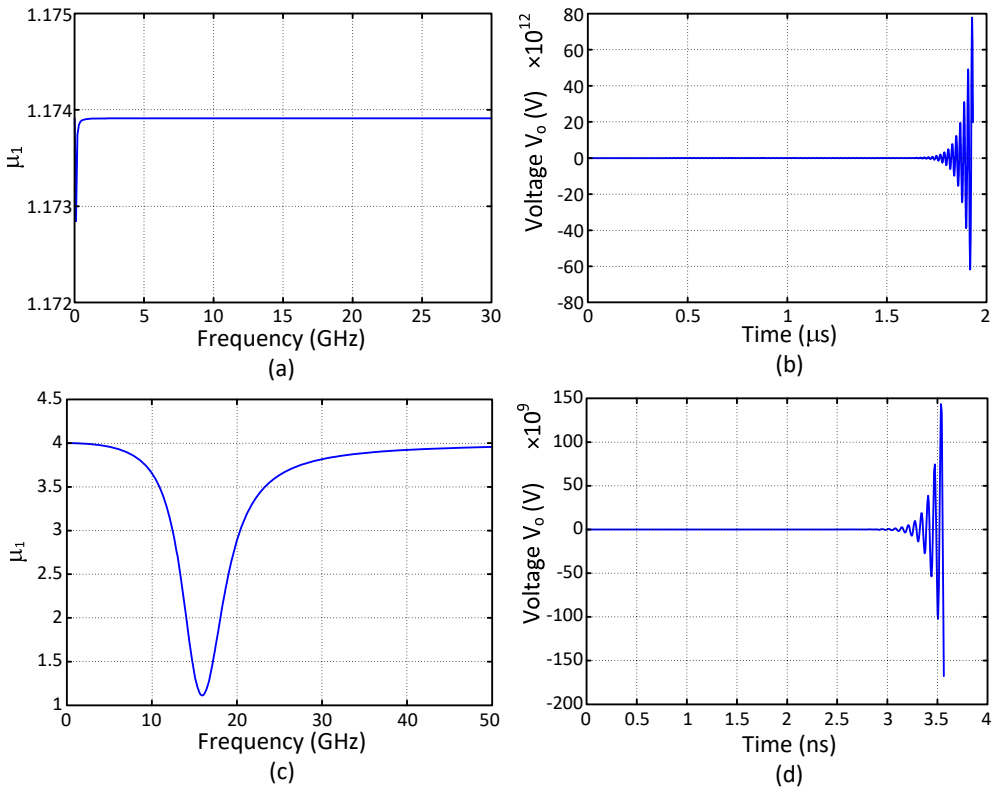

Fig. 5 Analysis of the circuits in Fig. 4. (a) and (b), μ factor and transient analysis of the circuit in Fig. 4(a). Initial condition V_o = 10 μV. (c) and (d), μ factor and transient analysis of the circuit in Fig. 4(b). Initial condition V_o = 100 μV.

Characteristic determinant

In most cases, instability of the dc solution leads the circuit to an oscillation, which can be physically explained as due to resonance with a negative resistance excess, employed in the transient growth of the oscillation amplitude. In 1968, Kurokawa published a very complete study of negative resistance oscillators [14], including mathematical conditions for the oscillation start-up from the noise level. The well-known conditions were derived for single resonator oscillators: only one inductor and only one capacitor. They can still be applied to circuits with more complex topologies, provided the circuit is analyzed at a suitable loop or node, with sufficient observability to detect the resonance responsible for the oscillation start-up. In a loop analysis, the total series impedance will be considered, whereas in a node analysis, the total parallel admittance is evaluated. In terms of total admittance $Y_T = G_T + jB_T$, the oscillation start-up conditions are given by:

$$\begin{aligned} &G_T(\omega_c) < 0 \\ &B_T(\omega_c) = 0 \\ &\frac{\partial B_T}{\partial \omega}(\omega_c) > 0 \end{aligned} \qquad (1)$$

The need for a positive sign in the frequency derivative of the susceptance is discussed later in the text. In general, the resonance frequency ω_c will not exactly agree with the steady-state oscillation frequency ω_o but will be close. The discrepancy can be understood from the nonlinear dependence of the susceptance, which should lead to zero large-signal value ($B_T = 0$) at a different frequency. An analogous condition in terms of the total impedance would detect an oscillation start-up due to an unstable series resonance. However, these evaluations of the oscillation start-up conditions rely on a partial single admittance (or impedance) analysis and may fail to predict instability in circuits with a complex topology. Evaluations of the total impedance when breaking the circuit at a particular loop or the total admittance at a particular

circuit node constitute just partial observations of this circuit that may be incapable of detecting internal instability mechanisms. How to proceed then?. The only way to obtain reliable information on the solution stability properties is to apply an accurate and complete stability analysis method.

The foundations of the stability analysis are better understood in time domain, which will be considered here only for conceptual reasons. In time domain [1-5] the number of state variables $x_1(t), x_2(t) \ldots x_N(t)$ is given by the highest time derivation order *N* required to describe the system. These state variables will be assembled in the vector $\overline{x}(t)$. They usually correspond to voltages across the capacitors and current through the inductors. To analyze the stability of the *dc* solution $\overline{x}_{dc}$ we will consider a small perturbation at the initial time only and analyze the circuit reaction to this perturbation. For stability, the small increment undergone by the variables, represented with the vector $\Delta\overline{x}(t)$, must exponentially decrease in time $\lim_{t\to\infty} \Delta\overline{x}(t) = 0$, so that the system returns to the original *dc* solution $\overline{x}_{dc}$. This analysis can be performed under a very convenient simplification. Because the perturbation must necessarily be small, we can linearize all the circuit nonlinearities elements about the *dc* solution $\overline{x}_{dc}$. This way the original nonlinear differential equation system becomes a much simpler linear differential equation system with constant coefficients, which in state form, can be compactly represented as $\Delta\dot{\overline{x}}(t) = [\mathrm{M}]\,\Delta\overline{x}(t)$, where [M] is a constant matrix [1-3]. With *N* state variables, the general solution of the linear system is [1]:

$$\Delta\overline{x}(t) = \sum_{k=1}^{N} c_k e^{\lambda_k t}\,\overline{u}_k = c_{c1}\, e^{(\sigma_{c1}+j\omega_{c1})t}\,\overline{u}_{c1} + c_{c1}^{*}\, e^{(\sigma_{c1}-j\omega_{c1})t}\,\overline{u}_{c1}^{*} + \mathrm{c}_{r1}\, e^{\gamma_{r1} t}\,\overline{u}_{r1} + \ldots \quad (2)$$

where the constant vectors $\overline{u}_k$ provide the independent directions of $\mathbb{R}^N$ in which the increment $\Delta\overline{x}(t)$ is decomposed, the constant coefficients c_k depend on the initial conditions $\Delta\overline{x}_o$, and the exponents λ_k, which can be real or complex conjugate, are the eigenvalues of [M]. Clearly, for stability we must have $\lim_{t\to\infty} \Delta\overline{x}(t) = 0$, which implies that all the λ_k must have negative real part or, equivalently, be located on the left-hand side of the complex plane (LHP). For any

positive real eigenvalue or any pair of complex-conjugate eigenvalues with positive real part, the increments undergone by the circuit variables will grow unboundedly in (2) and the *dc* solution will be unstable. Of course, the variables do not grow ad infinitum. What happens is that the system obtained by linearizing the nonlinear elements about the *dc* solution becomes invalid from certain amplitude of the system variables. This is why the linearization is unable to predict the steady-state solution to which the circuit evolves from the unstable *dc* solution.

As an example, the circuit in Fig. 6 will be analysed in the following. In this equivalent circuit, the nonlinear transconductance $i(v_1)$ has been linearized and replaced with $i(\Delta v_1) = g_m \Delta v_1$. The state variables will be the current through the inductor *L*, given by $\Delta i_L(t)$, and the voltages across the two capacitors C_1 and C_2, given by $\Delta v_1(t)$ and $\Delta v_2(t)$. This notation, making use of the increment symbol Δ, is preferred since the nonlinear function $i(v_1)$ has been linearized as $i(\Delta v_1) = g_m \Delta v_1$. Applying Kirchoff's laws, the circuit is governed by the following differential equation system:

$$\begin{aligned} \frac{d\Delta i_L}{dt} &= -\frac{1}{L}\Delta v_1 + \frac{1}{L}\Delta v_2 \\ \frac{d\Delta v_1}{dt} &= \frac{1}{C_1}\Delta i_L - \frac{G_1}{C_1}\Delta v_1 \\ \frac{d\Delta v_2}{dt} &= -\frac{1}{C_2}\Delta i_L - \frac{g_m}{C_2}\Delta v_1 - \frac{G_2}{C_2}\Delta v_2 \end{aligned} \qquad (3)$$

where $G_1 = 1/R_1$ and $G_2 = 1/R_2 + 1/R_3$. Clearly, the above system can be written in a matrix form as $\Delta\dot{\bar{x}}(t) = [\mathrm{M}]\,\Delta\bar{x}(t)$, where $\Delta\bar{x}(t) = [\Delta i_L(t), \Delta v_1(t), \Delta v_2(t)]^T$, T indicating transpose, and the matrix [M] is:

$$[\mathrm{M}] = \begin{bmatrix} 0 & -\frac{1}{L} & \frac{1}{L} \\ \frac{1}{C_1} & -\frac{G_1}{C_1} & 0 \\ -\frac{1}{C_2} & -\frac{g_m}{C_2} & -\frac{G_2}{C_2} \end{bmatrix}$$

The λ_k in (2) correspond to the eigenvalues of [M]. For $g_m = 0.2$ S, the three eigenvalues are $3.862\ 10^9 \pm j\,2\pi\ 10.569\ 10^9$ and $-9.201\ 10^{10}$, so the dc solution is unstable.

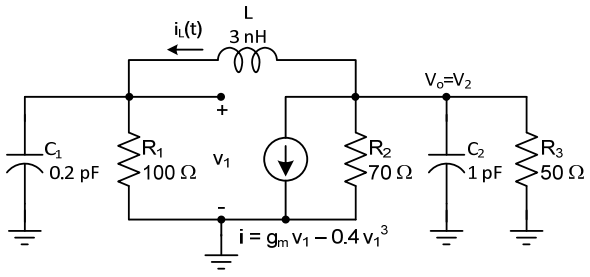

Fig. 6 Circuit containing a voltage controlled current source and a feedback element.

In principle, the eigenvalues λ_k can also be obtained from a frequency domain analysis of the circuit. To show this, a signal of the form $\Delta\bar{X}\ e^{st} = [\Delta I_L, \Delta V_1, \Delta V_2]^T e^{st}$, where *T* indicates transpose and *s* is a complex frequency, will be introduced into system (3). After simplifying the exponential terms, this provides the following system:

$$
\begin{aligned}
s\Delta I_L &= -\frac{1}{L}\Delta V_1 + \frac{1}{L}\Delta V_2 && \text{(a)} \\
s\Delta V_1 &= \frac{1}{C_1}\Delta I_L - \frac{G_1}{C_1}\Delta V_1 && \text{(b)} \qquad (4) \\
s\Delta V_2 &= -\frac{1}{C_2}\Delta I_L - \frac{g_m}{C_2}\Delta V_1 - \frac{G_2}{C_2}\Delta V_2 && \text{(c)}
\end{aligned}
$$

Clearly the above homogeneous system can be written in the form $\{sU - [\mathrm{M}]\}\Delta\bar{X} = 0$, where *U* is the identify matrix. The roots of the *characteristic determinant* $\det\{sU - [\mathrm{M}]\} = 0$ agree with the eigenvalues λ_k, confirming that they can be calculated through a frequency-domain analysis of the system. It is also interesting to note that these eigenvalues can also be obtained if we reduce number of system equations by substitution. Solving (4)(b) and (4)(b) for ΔI_L and ΔV_2 in terms of ΔV_1, and replacing into (4)(a), one obtains:

$$
\left[1 + \frac{1}{LC_1C_2s^3 + (G_2LC_1 + G_1LC_2)s^2 + (C_1 + C_2 + G_1LG_2)s + G_1 + G_2}\, g_m\right]\Delta V_1 = 0 \qquad (5)
$$

This example illustrates how it is possible to reduce the number of equations at the expense of a higher order in the frequency *s*. Indeed, system (4) is composed by three first order equations in *s*, whereas (5) contains a single equation of third order in *s*.

In the following, a general formulation for the stability analysis of *dc* solutions, applicable to circuits with arbitrary topology, will be presented. It is derived from a harmonic-balance formulation of the piecewise type [10,20], which is more compact than the nodal one [4] since it uses a smaller set of state variables. The relationship between the two formulations is analogous to the one existing between the two equivalent analyses presented for circuit in Fig. 6, the one based on (4), with three state variables, and the one in (5), with only one state variable.

The circuit partitioning in the piecewise harmonic-balance formulation is sketched in Fig. 7. In the common case of a circuit without nonlinear fluxes, the state variable of this formulation will be the control voltages of the nonlinear current sources and charges, corresponding to the voltages $v_1(t)\ldots v_P(t)$ in Fig. 7. The harmonic components of this set of state variables will be ranged into a vector $\overline{V}$. We will have another set of elements, constituted by the nonlinear functions controlled by $v_1(t)\ldots v_P(t)$. These functions can be nonlinear currents and nonlinear charges, respectively corresponding to $i_1\ldots i_M$ and $q_1\ldots q_L$ in Fig. 7. The dependence of these purely nonlinear functions on their control voltages is defined in time domain, through instantaneous relationships. This is a fundamental characteristic of the harmonic balance method, which relies on the natural time-domain description of the nonlinear elements. Note that any linear element of the device models will be included in the global linear embedding network. For the frequency domain analysis, the harmonic components of all the nonlinear currents and charges will be ranged in another vector $\overline{I}$. The dependence of this vector on the control voltages will be expressed, in a general manner as $\overline{I}(\overline{V})$. The circuit will also have independent sources $e_{g1}\ldots e_{gR}, i_{g1}\ldots i_{gS}$, which will be ranged, at their corresponding frequencies, in a vector $\overline{G}$.

After defining these three vectors, $\overline{V}$, $\overline{I}(\overline{V})$ and $\overline{G}$, one must take into account that, in the circuit operation, the components of these vectors will be connected through the mentioned linear network (as sketched in Fig. 7) at each of the analysis frequencies. Thus, the vector $\overline{I}$

will have a double dependence on the state variables $\overline{V}$: through the instantaneous characteristics of the nonlinear elements , providing $\overline{I}(\overline{V})$, and through the linear network, which will also account for the influence of the input generators $\overline{G}$.

Application of Kirchoff's laws to the linear network (by simply considering the components of $\overline{I}(\overline{V})$ as voltage-controlled current sources and capacitances) at each of the harmonic frequencies leads to the following system, expressed in matrix form:

$$\overline{V} + \left[Z(\omega)\right] \overline{I}(\overline{V}) + \left[Z_G(\omega)\right]\overline{G} = \overline{0} \qquad (6)$$

where $\left[Z(\omega)\right], \left[Z_G(\omega)\right]$ are linear matrixes, obtained through evaluation of the passive linear network. To avoid excessive mathematical detail, a general dependence on ω is considered. In fact, in the harmonic-balance analysis of periodic (or quasi-periodic) solutions, the compact system (6) will decompose into several coupled subsystems, one at each frequency ω_k considered in the Fourier series. The coupling will be due to the dependence of the nonlinear elements on all the harmonic components of the control voltages.

The piecewise formulation in (6) will be used to derive the formulation used for the small-signal stability analysis. As already stated, this depends only on the stability properties of the *dc* solution, so all the small signal generators can be set to zero. Thus, the only components different from zero in the vector $\overline{G}$ will be those corresponding to the *dc* sources, and system (6) will provide the *dc* solution that will be the object of the stability analysis. For this analysis, a small perturbation will be applied. Because the perturbation is small, we can linearize the nonlinear elements about the *dc* solution. This implies, for instance, replacing the nonlinear transconductance function of FET devices with the linear model about the particular *dc* operation point, in terms of $g_m = \partial i_{ds} / \partial v_{gs}$, $g_{ds} = \partial i_{ds} / \partial v_{ds}$. See for instance the linearization $i(\Delta v_1) = g_m \Delta v_1$, considered in the circuit of Fig. 6. In the formalism (6) that is being used here, we will have a matrix composed by the derivatives of all the nonlinear elements with respect to the control voltages, which will be represented as $\partial \overline{I} / \partial \overline{V}\big|_{DC}$. Another essential fact is that the passive frequency-dependent components must be evaluated at a complex frequency *s*. Reason

for this is that we are not analyzing a steady-state regime (for which the frequency would be real) but evaluating a perturbation transient, with a solution of the form (2). Proceeding as described, one would obtain a system expressible in the following form [10,20]:

$$\Delta\bar{V} + [Z(s)] \left.\frac{\partial \bar{I}}{\partial \bar{V}}\right|_{DC} \Delta\bar{V} = \left\{ [U] + [Z(s)] \left.\frac{\partial \bar{I}}{\partial \bar{V}}\right|_{DC} \right\} \Delta\bar{V} = 0 \qquad (7)$$

where $\Delta\bar{I}$ are the increments in the nonlinear currents and *charges*, $\Delta\bar{V}$ are the increments of control voltages and matrix [Z(s)] accounts for the linear relationships between $\Delta\bar{V}$ and $\Delta\bar{I}$, obtained through the evaluation of the circuit passive network. Note that the whole system (7) is equated to zero since there are no sources at the perturbation frequency *s*. The matrix $[Z(s)]$ provides the relationship $\Delta\bar{V} = -[Z(s)]\,\Delta\bar{I}$ between $\Delta\bar{V}$ and $\Delta\bar{I} = \left.\frac{\partial \bar{I}}{\partial \bar{V}}\right|_{DC} \Delta\bar{V}$, calculated by considering the linear part of the circuit only. Therefore, the matrix $[Z(s)]$ has a "feedback effect" [6].

To have $\Delta\bar{V}$ different from zero, the matrix affecting this vector must be singular. The associated determinant, termed *characteristic determinant* [10,15,20] must be equal to zero:

$$\det(s) = \det\left\{ [U] + [Z(s)] \left.\frac{\partial \bar{I}}{\partial \bar{V}}\right|_{DC} \right\} = 0 \qquad (8)$$

Note that the order of the characteristic determinant (8) must agree with the order *N* of the time-domain system, as in the two formulations (4) and (5). Moreover the roots of (8) agree with the eigenvalues λ_k in (2), since they are independent of the choice of the state variables.

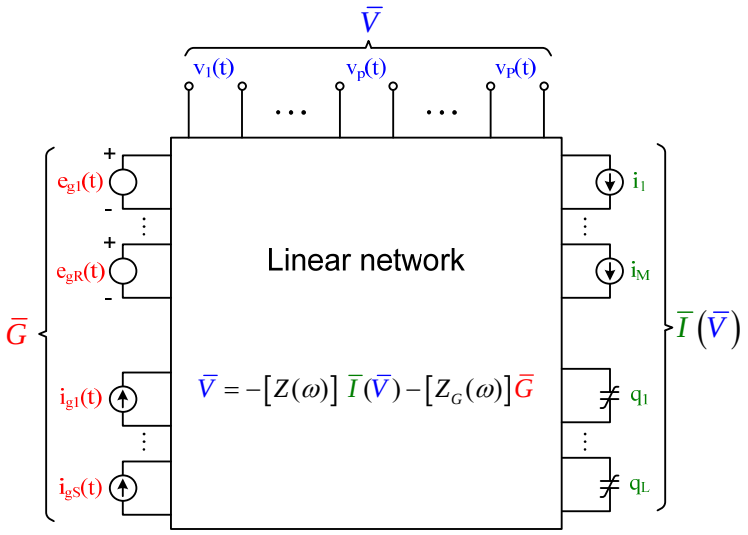

Fig. 7 Circuit partitioning in *piecewise* harmonic balance. There are three sets of elements: control voltages, nonlinear elements depending on these voltages and independent generators. The vectors are composed by the harmonic components of these elements. The linear embedding network connects the components of the three vectors at each of the analysis frequencies.

The above methodology has been applied to the simple circuit in Fig. 6. The active element is a voltage controlled current source $i(v)$ that has been linearized about the *dc* solution and therefore is modelled as $\Delta I = g_m \Delta V_1$, where ΔV_1 is the control voltage. The function $Z(s)$ in (7) relates the control voltage ΔV_1 to the controlled current ΔI. Therefore it can be seen as a transfer function from ΔI to ΔV_1. Using the formalism (8), one obtains exactly the same equation in (5), which can be rewritten in a compact manner, as:

$$1 + Z(s)\left.\frac{\partial \bar{I}}{\partial \bar{V}}\right|_{DC} = 1 + Z(s)\, g_m = 0 \qquad (9)$$

Because there is only one state variable, the dimension of the characteristic system is one and system (9) agrees with the characteristic determinant. By solving (9), one obtains the singularities associated with the *dc* solution, which determine the transient reaction to perturbations according to the general expression (2).

The results obtained for three values of the linear transconductance g_m are shown in Table II. Because the system dimension is 3 there are three roots of (5) or equivalently three

eigenvalues in (2). For g_m = 0.1 S, the three eigenvalues have negative real part and the circuit is stable. For g_m = 0.1435 S, there is a significant reduction of the real part of the complex conjugate eigenvalues at 9.7 GHz. The poles are nearly on the imaginary axis when represented in the complex plane, which implies operation near a qualitative stability change or *bifurcation*. For g_m = 0.2 S, the pair of complex conjugate poles has positive real part, which indicates unstable behaviour. For that g_m value, an oscillation starts up at 10.6 GHz.

Table II Eigenvalues of the circuit in Fig. 6 for different g_m.

g_m (S)	$\sigma \pm \mathrm{j}\omega_o/(2\pi)$	γ
0.1	$-3.78\ 10^9 \pm \mathrm{j}\ 8.89\ 10^9$	$-7.673\ 10^{10}$
0.1435	$-3.93\ 10^6 \pm \mathrm{j}\ 9.699\ 10^9$	$-8.428\ 10^{10}$
0.2	$3.862\ 10^9 \pm \mathrm{j}\ 10.569\ 10^9$	$-9.201\ 10^{10}$

The analysis based on (8) provides all the circuit natural frequencies or eigenvalues λ_k. In comparison, the oscillation start-up conditions (1) directly check [5] for the possible existence of a pair of dominant complex-conjugate eigenvalues $\sigma \pm j\omega_o$, located in the right hand side of the complex plane (RHP). The RHP location of this pair of complex-conjugate eigenvalues requires a positive value of the frequency derivative of the susceptance [5] at the resonance frequency, as imposed in (1). Unlike conditions (1), the characteristic determinant (8) globally takes into account all the circuit dynamics, as it does not depend on any observation port or node. However, resolution of (8) in terms of the complex frequency s is an arduous problem in high order systems. Several alternative numerical methods have been proposed to avoid this direct resolution.

Nyquist analysis of the characteristic determinant

In 1985, the work [15] proposed the application of Nyquist criterion to the determinant function $\det(s)$ in (8). The Nyquist criterion relies on a crucial property [12] of any linear complex function of a complex variable s, denoted by $F(s)$, named *argument principle*. The complex function $F(s)$ must tend to zero or a constant value in the limit $s \to \infty$. Consider the plot

resulting from evaluating $F(s)$ along a closed contour Γ of the complex plane, in a clockwise sense [12]. This plot must not pass through any zero or pole of $F(s)$. Then the number (N_T) of clockwise encirclements of the plot $F(\Gamma)$ around the origin of the complex plane is equal to the difference between the number of zeroes (Z) and poles (P) of the complex function F, contained inside the contour Γ, that is, $N_T = Z - P$.

For the stability analysis of a circuit dc solution, the complex function considered is $F(s) = \det(s)$, that is, the characteristic determinant in (8). We want to determine the number of zeroes of this function located on RHP, which agrees with the solution poles. This region of the plane is bounded by the entire imaginary axis $j\omega$ and a semi-circular trajectory of infinite radius $s \to \infty$. Note that for the application of the Nyquist criterion to $\det(s)$, this function must tend to zero or a constant value for $s \to \infty$, which must be satisfied by (8). Thus, it will be sufficient to evaluate $\det(s)$ along the imaginary axis $j\omega$, with ω going from $-\infty$ to ∞, calculating $\det(j\omega)$. The determinant is clearly complex since terms at $-j\omega$ are not included in the calculation. The Nyquist plot is obtained by sweeping ω and tracing $\mathrm{Im}\{\det(j\omega)\}$ versus $\mathrm{Re}\{\det(j\omega)\}$. As already stated, the number of clockwise encirclements of the origin is $N_T = Z - P$. However, the poles of (8) can only come from the matrix $[Z(s)]$ which due to its passivity [15] cannot introduce any unstable poles in the determinant function $\det(s)$. Note that this matrix originates from the evaluation of impedances and/or admittances of the passive linear elements. However, the function $\det(s)$ can have RHP roots (corresponding to unstable circuit poles), which would come from the multiplication of $[Z(s)]$ by the linearized device matrix $\partial\bar{I} / \partial\bar{V}\big|_{DC}$.

Because of the absence of RHP poles of the determinant function, the number N of clockwise encirclements around the origin of the complex function $\det(j\omega)$, evaluated from $\omega = -\infty$ to $\omega = \infty$, will directly provide the number Z of unstable roots of $\det(s)$. This is not true when using other functions, such as the total admittance from a given observation node

(1) or total impedance through a given observation loop. Those functions may have both zeroes and poles on the RHP, since due to the variable reduction in the calculation of the current-to-voltage or voltage-to-current functions, coefficients associated with the device linearization will affect both the numerator and denominator. This is why the use of the total immittance functions may fail to predict instability.

As an example, the Nyquist stability analysis described above has been applied to the *dc* solution of the circuit in Fig. 6. The complex function used in the Nyquist plot is obtained by replacing the complex frequency *s* with $j\omega$ in (5):

$$\det(j\omega) = \left[1 + \frac{1}{LC_1C_2(j\omega)^3 + (G_2LC_1 + G_1LC_2)(j\omega)^2 + (C_1 + C_2 + G_1LG_2)(j\omega) + G_1 + G_2} g_m \right] \quad (10)$$

The imaginary part of $\det(j\omega)$ is then traced versus the real part (see Fig. 8). Because of the Hermitian symmetry of the frequency domain system, the function $\det(j\omega)$ is symmetrical (complex conjugate) for $\omega > 0$ and $\omega < 0$, so it is sufficient to consider positive ω. The analysis has been performed for several values of the linear transconductance g_m, sweeping the perturbation frequency from zero to 25 GHz. As can be seen, for $g_m < 0.1435$ S, the plot does not encircle the origin and the circuit is stable, due to insufficient gain. For $g_m > 0.1435$ S, the plot encircles the origin and the circuit is unstable. At the critical value $g_m = 0.1435$ S, the circuit undergoes a qualitative change of stability. This corresponds to a Hopf bifurcation, in which a pair of complex-conjugate poles crosses the imaginary axis to the RHP, giving rise to an oscillation.

The frequency ω_c at which the Nyquist plot crosses the negative real semi-axis provides an estimation of the oscillation frequency. For instance, with the transconductance value $g_m = 0.1435$ S, the crossing frequency is $f_c = 9.7$ GHz. The steady-state oscillation frequency calculated with time domain integration is $f_o = 9.55$ GHz. The similarity in these frequency values is in close relationship with the fact that at the steady-state oscillation, the Jacobian matrix of the harmonic-balance system is singular and fulfills $\mathrm{Re}\{\det(j\omega_o)\} = 0$ and $\mathrm{Im}\{\det(j\omega_o)\} = 0$ [5-6,15]. The singularity is due to the invariance of the oscillator solution

with respect to changes in the phase origin [1,5,6,10]. Because the imaginary part mostly depends on the reactive elements, with most of them being linear, the frequency ω_c at which $\mathrm{Im}\{\det(j\omega_c)\}=0$ is fulfilled will be relatively close to the actual oscillation frequency ω_o. These results have been validated with time-domain integration. The transient simulations for $g_m = 0.1$ S, $g_m = 0.1435$ S (very close to the bifurcation point) and $g_m = 0.2$ S are shown in Fig. 9. The proximity to the bifurcation point [Fig. 9(b)] is characterized by a slow transient response associated with the small magnitude of the real part σ of the dominant pair of complex-conjugate poles.

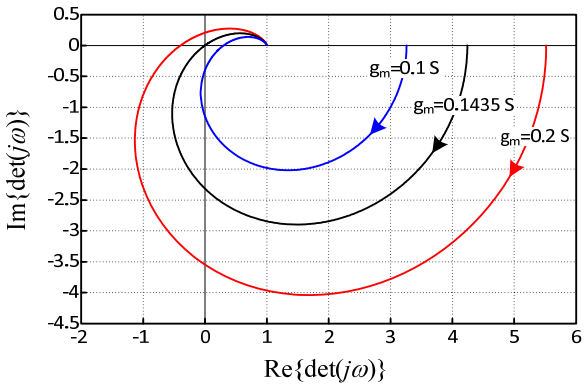

Fig. 8 Stability analysis of the circuit in Fig. 6 based on the application of the Nyquist criterion to the characteristic determinant of the harmonic-balance system, linearized about the *dc* solution. It is stable for $g_m <$ 0.1435 S, unstable for $g_m >$ 0.1435 S and undergoes a Hopf bifurcation for g_m = 0.1435 S.

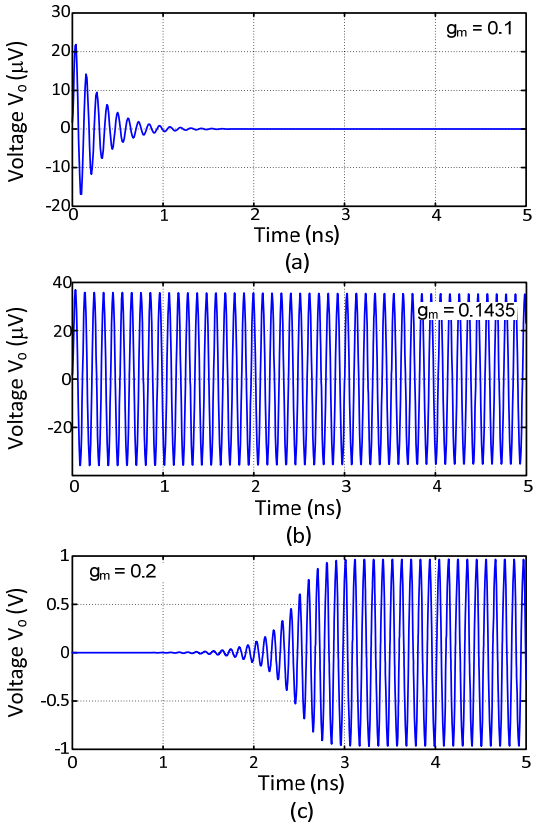

Fig. 9 Time domain analysis of the circuit in Fig. 7. The results agree with those predicted by the Nyquist analysis in Fig. 8. (a) $g_m = 0.10$ S, stable. Oscillation extinction. (b) $g_m = 0.1435$ S, near bifurcation. (c) $g_m = 0.2$ S, unstable, with oscillation start-up.

Normalized determinant function

The Nyquist stability analysis applied to the characteristic determinant (8) relies on the full computation of the device linearization matrix $\partial\overline{I} / \partial\overline{V}\big|_{DC}$, which is not available in commercial harmonic balance simulators. An alternate technique proposed in [25-26] enables an indirect calculation of the determinant $\det(j\omega)$ from open-loop functions that can be obtained with commercial software. To enlighten the possibility to obtain this normalized version from an evaluation of open-loop transfer functions, just note that in the case of a single nonlinearity and a single control voltage, the left-hand side of equation (7) would be formally identical to the denominator of the transfer function of a feedback loop [12]: $H(s) = A / (1 - AB)$, where A and B are the direct and feedback transfer functions, respectively. The so-called *return ratio* is defined

by $RR = -AB$ [25-26]. In terms of the return ratio RR, the denominator of the closed-loop transfer function $H(s)$ is given by: $F = 1 + RR$. Still considering a single active element, a voltage-controlled current source, for instance, the functions $Z(s)$ and $\partial\overline{I} / \partial\overline{V}\big|_{DC}$ would play the role of A and B. The product $Z(s)\left(\partial\overline{I} / \partial\overline{V}\big|_{DC}\right)$ constitutes the open-loop transfer function of the system. When the loop is closed, the control voltage V constitutes both the system input and output.

The calculation of the NDF is intended for later application of the Nyquist criterion [25-26]. Therefore, it will be calculated in terms of $j\omega$ instead of the complex frequency s. To obtain the open loop transfer function of the circuit in Fig. 6, the closed loop is broken, making the current depend on an external voltage V_{ext}, and obtaining the voltage drop at the original location of the control voltage $\Delta V_1'$ [Fig. 10]. The open loop circuit is formulated as:

$$\Delta V_1' + \frac{1}{LC_1C_2(j\omega)^3 + (G_2LC_1 + G_1LC_2)(j\omega)^2 + (C_1 + C_2 + G_1LG_2)(j\omega) + G_1 + G_2} g_m V_{ext} = \\ = \Delta V_1' + Z(j\omega)\, g_m\, V_{ext} = 0 \qquad (11)$$

So the open loop transfer function is given by:

$$-RR = \frac{\Delta V_1'}{V_{ext}} = -Z(j\omega)\, g_m \qquad (12)$$

And the so called Normalized Determinant Function, calculated as $NDF = 1 + RR(j\omega)$, fully agrees with the Nyquist function $\det(j\omega)$ in (10).

Note that the feedback formulation used in (7) is not the only possible one to derive the circuit characteristic system. For instance, we could have analyzed the circuit using 2x2 admittance matrixes to describe the active element and the passive network, using a formulation of the type:

$$\left[Y_T(s)\right]\Delta\overline{V} = \left\{\begin{bmatrix} 0 & 0 \\ -g_m & 0 \end{bmatrix} + \begin{bmatrix} Y_{11}(s) & Y_{12}(s) \\ Y_{21}(s) & Y_{22}(s) \end{bmatrix}\right\} \begin{bmatrix} \Delta V_1 \\ \Delta V_2 \end{bmatrix} = 0 \qquad (13)$$

And the associated characteristic determinant is that of the matrix on the left-hand side of (13). Unlike (7) the above formulation is not normalized. The function $NDF = 1 + RR$ agrees with the

normalized determinant, or ratio between the characteristic determinant $\det(s)$ obtained with any formulation [such as (13)] and the determinant obtained when the active elements are switched off, $\det_o(s)$. Applying this to the particular formulation in (13), one obtains:

$$NDF = \frac{\det(s)}{\det_o(s)} = \frac{g_m Y_{12}(s) + Y_{11}(s)Y_{22}(s) - Y_{12}(s)Y_{21}(s)}{Y_{11}(s)Y_{22}(s) - Y_{12}(s)Y_{21}(s)} = \\ = 1 + \frac{g_m Y_{12}(s)}{Y_{11}(s)Y_{22}(s) - Y_{12}(s)Y_{21}(s)} = 1 + Z(s) g_m = 0 \quad (14)$$

In the case of multiple active elements, obtaining the normalized determinant function NDF is more involved. In fact, the NDF calculated by opening the circuit at just one single active element can contain poles on the RHP [25-26]. To illustrate this, we will consider M independent active devices of transconductance type, g_{m1} … to g_{mM}, each depending on its own control voltage. Then the characteristic system can be written as:

$$\begin{bmatrix} \Delta V_1' \\ \Delta V_2 \\ \vdots \\ \Delta V_M \end{bmatrix} + \begin{bmatrix} z_{11}(j\omega) & z_{12}(j\omega) & \cdots & z_{1M}(j\omega) \\ z_{21}(j\omega) & z_{22}(j\omega) & \cdots & z_{2M}(j\omega) \\ \vdots & \vdots & \cdots & \vdots \\ z_{m1}(j\omega) & z_{m2}(j\omega) & \cdots & z_{MM}(j\omega) \end{bmatrix} \begin{bmatrix} g_{m1} & 0 & \cdots & 0 \\ 0 & g_{m2} & \cdots & 0 \\ \vdots & \vdots & \cdots & \vdots \\ 0 & 0 & \cdots & g_{mM} \end{bmatrix} \begin{bmatrix} V_{ext} \\ \Delta V_2 \\ \vdots \\ \Delta V_M \end{bmatrix} = 0 \quad (15)$$

Clearly, the open loop transfer function $-RR = \frac{\Delta V_1'}{V_{ext}}$ obtained through resolution of the above linear system may contain poles on the RHP, resulting from the action of the transconductances g_{m2} … to g_{mM}. Therefore, we cannot apply the Nyquist plot to the function 1+*RR*, due to the possible existence of both RHP zeroes and poles. Note that in these conditions the number of encirclements around the origin of the Nyquist plot, agreeing with $N = Z - P$, would not be conclusive.

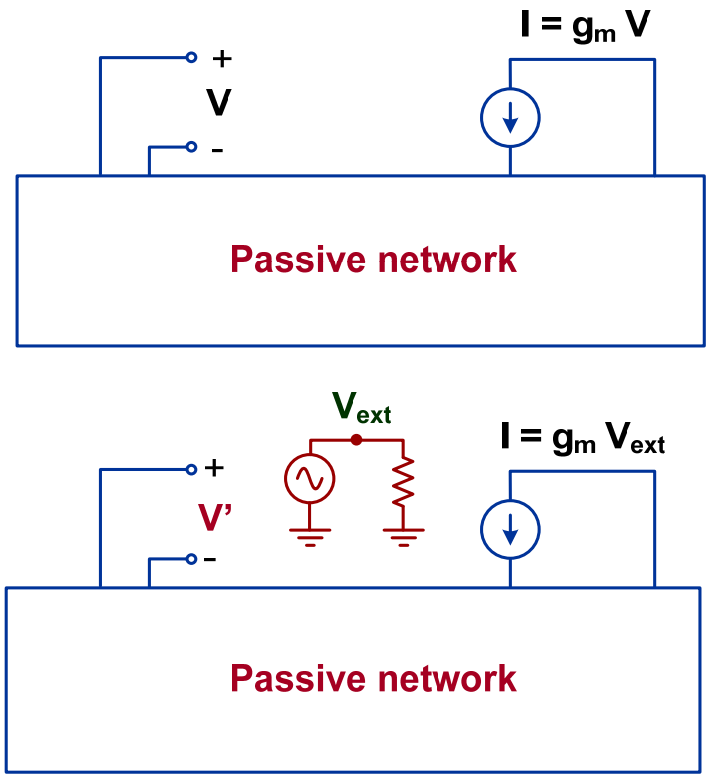

Fig. 10 Circuit analysis in open-loop conditions for the determination of the return ratio. (a) Original circuit containing a single active device. (b) After opening the loop, the ratio V'/V_{ext} provides the open-loop transfer function $-RR = V'/V_{ext}$. The return ratio is given by RR.

The works [25-26] have demonstrated that in the presence of multiple active devices, the determinant in (8) can be calculated by recursively obtaining M open-loop transfer functions, with the M active elements in different operation conditions. The calculation [25-26] starts by obtaining the return ratio associated with the first active element RR_1. This is calculated by breaking the loop associated with this controlled element, as in the single-element case, and keeping the rest of the active elements 2 to M in nominal operation. Then the return ratio RR_2 associated with the second active element is calculated with the second active element in open loop conditions, doing $-RR_2 = \Delta V_2'/V_{ext}$, where $\Delta V_2'$ is the voltage across this element when it is made depend on the external voltage V_{ext} instead of the actual control voltage ΔV_2. The return ratio RR_2 is calculated by turning off the first active element and keeping elements 3 to M in nominal operation. The recursive calculation of return ratios finalizes with RR_M, obtained with

all the previous active elements 1 to *M*-1 switched off and the last active *M* in open loop conditions. It can be analytically demonstrated [25-26] that the normalized determinant function can be calculated as:

$$NDF(j\omega) = (1 + RR_1)(1 + RR_2)...(1 + RR_M) \tag{16}$$

The NDF can be evaluated in commercial software from the determination of the return-ratio functions RR_1 to RR_M, which requires access to all the different active elements that must alternatively be in nominal operation, open-loop configuration and turned off.

The analysis based on the NDF has been applied to the circuit in Fig. 11, containing two nonlinear transconductances. The Nyquist plots obtained with $g_m = 0.25$ S, $g_m = 0.30$ S and $g_m = 0.35$ S are shown in Fig. 12. For $g_m = 0.25$ S the plot does not encircle the origin, so all the circuit poles should be located on the LHP. For $g_m = 0.30$ S the plot crosses through the origin, which corresponds to a bifurcation condition (limit stability situation). For $g_m = 0.35$ S, the plot encircles the origin in clockwise sense, this indicating instability with a pair of complex-conjugate poles at a frequency near the one at which the plot crosses the negative real semi-axis. For $g_m > 0.35$ S, an oscillation starts up from the noise level (Fig. 13). The oscillation is odd mode, that is, there is 180º phase shift between the two circuit branches. The odd mode oscillation is potentiated by the circuit symmetry since in these conditions the branching nodes become virtual short circuits, which reduces the positive resistance seen from the device terminals.

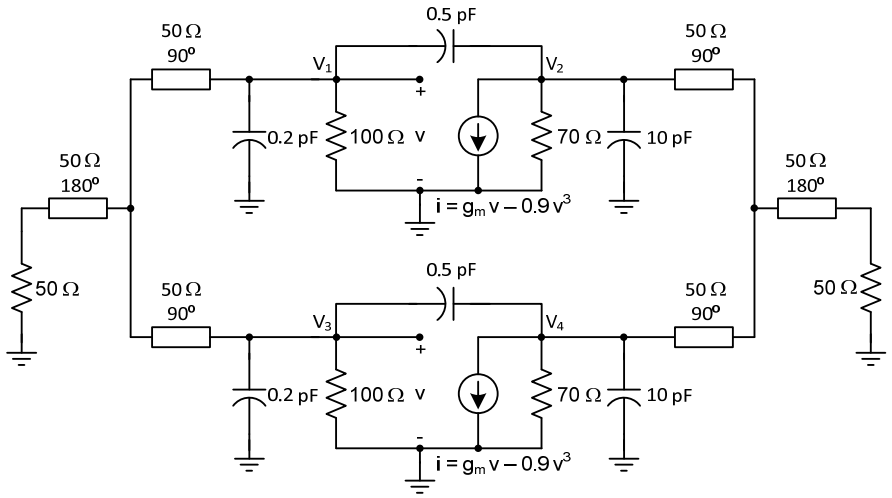

Fig. 11 Circuit containing two active devices and feedback elements in a power-combining topology.

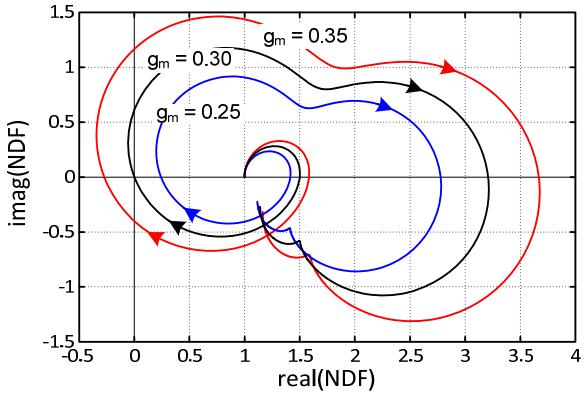

Fig. 12 Application of the normalized determinant function (NDF) to the circuit in Fig. 11. Nyquist plots. (a) $g_m = 0.25$ S. Stable. (b) $g_m = 0.30$ S. Hopf bifurcation. (c) $g_m = 0.35$ S. Unstable.

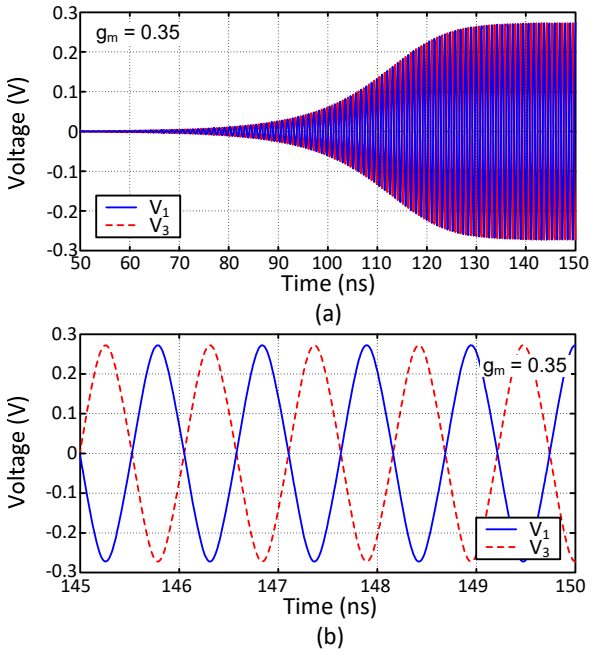

Fig. 13 Time domain analysis of the circuit in Fig. 11 for $g_m = 0.35$ S. (a) Transient. (b) Steady state showing an odd mode oscillation.

Pole-zero identification

A transfer function of a given linear system is defined as the ratio between a particular system output and input when all the system initial conditions are zero. By control theory [12], all the closed loop transfer functions that can be defined in a linear system (such as the circuit

linearized about a particular *dc* solution) share the same denominator, and, as will be shown, this denominator agrees with the system characteristic determinant. The works [28-31] proposed the application of pole-zero identification to a *closed-loop transfer function* obtained by linearizing the circuit about the examined *dc* solution.

Assume that a small-signal input current source I_n at the frequency ω is introduced into the circuit. Due to the small amplitude of the current generator, the nonlinear devices can be linearized about the *dc* solution, as in the case of the stability analysis based on (7). This provides the linear system:

$$\left\{ \left[U\right] + \left[Z(j\omega)\right] \left. \frac{\partial \bar{I}}{\partial \bar{V}} \right|_{DC} \right\} \Delta \bar{V} = -\left[Z_G(j\omega)\right] I_n \tag{17}$$

where $[Z_G]$ is the column matrix relating the circuit variables to the current generator I_n. In (7), the perturbation was applied at the initial time only, so it does not appear in the linearized equation. In (17), a small-signal sinusoidal generator I_n is permanently connected to the circuit, which behaves linearly with respect to this generator.

As already stated, whatever input is connected to a linear system, all the possible transfer functions share the same denominator, which depends only on the system itself, instead of the particular location or nature of the input and output signals. This can be gathered from inspection of (17). The calculation of any possible transfer function S_{out}/I_n, where S_{out} is an arbitrary output, requires the inversion of the matrix on the left-hand side. This matrix is formally identical to the one analyzed in (7) for the determination of the system singularities. Actually, the matrix in (17) is obtained by simply doing $s = j\omega$ in (7). For the definition of the transfer function, a very convenient output (for reasons of numerical accuracy) is the voltage V_n at the node where the current generator is connected [28-31]. Thus, the transfer function considered is:

$$Z_{in}(j\omega) = \frac{V_n(j\omega)}{I_n(j\omega)} \tag{18}$$

Using pole-zero identification, the complex function $Z_{in}(j\omega)$ is fitted through a least squares technique, with a quotient of polynomials of the form [28,31]:

$$Z_{in}(j\omega) = \frac{V_n}{I_n}(j\omega) = A\frac{(j\omega - z_1)\ \ldots(j\omega - z_m)}{(j\omega - p_1)\ \ldots(j\omega - p_n)} \tag{19}$$

Note that the zeroes and poles of $Z_{in}(s)$ depend on the constants $z_1 \ldots z_m$ and $p_1 \ldots p_n$, as the Z_{in} expression would be formally identical in terms of *s*. The pole-zero identification should be performed between $\omega \cong 0$ and the frequency ω_{max}. Accurate identification in a very wide frequency interval may require a high order *n* of the polynomial in the denominator of (19), so the quality of the identification thus may degrade. As a matter of fact, the required order would be theoretically infinite in the case of circuits containing distributed elements. However, because the transfer function $Z_{in}(j\omega)$ is linear, the total frequency interval 0 to ω_{max} may be divided into sub-intervals, which will allow an accurate identification using a smaller order *n* in the denominator of (19).

As already stated, all the closed-loop transfer functions that can be defined in a given linear system share the same denominator [28-31]. In contrast, the numerator depends on the particular definition of the transfer function. Thus, it will depend on the node selected for the connection of the current source. Because of this, cancellations of unstable poles with zeroes in the RHP may take place at some particular locations. If unstable poles are cancelled, a wrong conclusion about the stability of the solution may be obtained. This is why the pole-zero identification should be performed for different locations of the current source. The terminal nodes of the active devices are the most convenient for this analysis, due to their proximity to the potential "sources" of instability. Although the case of a current source connected in parallel has been considered, the technique is equally applicable with a voltage source V_n in a series connection, using an admittance transfer function $Y_n = I_n / V_n$. As shown in [30], the admittance type transfer function is more convenient if there is a passive impedance of small value, dominating the impedance coming from the active part, where instability occurs. Note that the possible existence of zeroes in the RHP does not have any implication for system stability. If a

transfer function has poles and/or zeros in the RHP, then the system shows *non-minimum phase behaviour* [12].

The transfer function (19) exactly agrees with the inverse of the total input admittance at the node *n* where the current source is introduced, namely $Y_{in}(j\omega) = I_n(j\omega)/V_n(j\omega)$. Assuming that $Y_{in}(\omega)$ is evaluated at a sensitive location, it is possible to relate the oscillation start-up conditions [see (1)] derived by Kurokawa $G_{in}(\omega_c) < 0, B_{in}(\omega_c) = 0$, $\partial B_{in}(\omega_c)/\partial\omega > 0$ to the existence of a pair of unstable complex-conjugate poles in the closed-loop transfer function $Z_{in}(j\omega)$ [inverse of $Y_{in}(j\omega)$], as has been shown in [5]. The dual is true for an analysis based on the series connection of a voltage generator in terms of the input impedance.

Pole-zero identification has been applied to the circuit in Fig. 11. To calculate a closed-loop linear transfer function, a small-signal current source $I_n(\omega)$ is connected in parallel at node 2. The stability analysis of the dc solution with g_m = 0.35 S provides the pole-zero locus of Fig. 14(a). The frequency interval considered to obtain this particular locus is 0 to 10 GHz. The stability has also been analyzed versus the linear coefficient of the transconductance function g_m. For each g_m value, two different analyses are performed. The first analysis provides the dc solution. The second is a small-signal analysis in which the frequency ω of the current source is swept to obtain the transfer function $Z_{in}(j\omega)$. Pole-zero identification is applied to each of the functions $Z_{in}(j\omega)$ obtained in this manner. In Fig. 14(b) the real part of the dominant poles (the ones with largest real part σ) of $Z_{in}(s)$ has been traced versus the linear transconductance coefficient g_m.

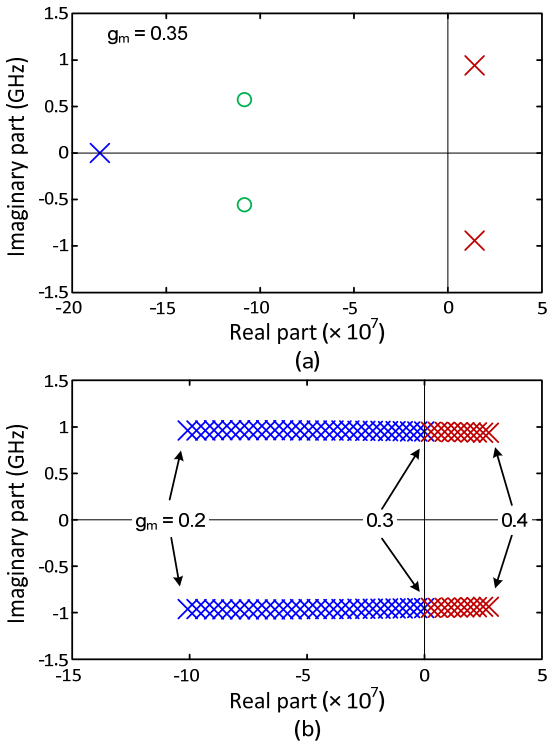

Fig. 14 Stability analysis of the dc solution of the circuit in Fig. 11 using pole-zero identification. (a) Pole-zero locus for g_m = 0.35 S. (b) Evolution of the dominant pair of complex-conjugate poles versus g_m.

Stability analysis of a periodic solution

As already stated, the so-called *small signal instability* is due to the instability of the circuit *dc* solution, since the circuit behaves linearly with respect to the small-signal input sources and, therefore, these sources cannot have any impact on the stability properties of the *dc* solution. In contrast, the *large signal stability* analysis (in circuits depending nonlinearly on the time-varying input sources) must be addressed taking into account the effect of these input sources [5-7,15-16,20]. All the stability analysis methods described for the stability analysis of *dc* solution have an extension for the case of periodic regimes. The main difference is that in the case of a large-signal periodic regime, one must take into account the combined effect of steady-state frequency ω_o and the complex perturbation frequency s, coming from noise or fluctuations. Due to the "mixing" between these two frequencies, the general expression of the perturbation, in time domain, is the following [1-3]:

$$\Delta\overline{x}(t) = \sum_{k=1}^{N} c_k e^{\lambda_k t}\,\overline{u}_k(t) = c_{c1}\, e^{(\sigma_{c1}+j\omega_{c1})t}\,\overline{u}_{c1}(t) + c_{c1}^{*}\, e^{(\sigma_{c1}-j\omega_{c1})t}\,\overline{u}_{c1}^{*}(t) + c_{r1}\, e^{\gamma_{r1} t}\,\overline{u}_{r1}(t) + \ldots \quad (20)$$

where N agrees with the number of reactive elements. The complex vectors $\overline{u}_k(t)$, $k = 1$ to N, are periodic with the same period $T = 2\pi/\omega_o$ as the periodic solution, and the complex exponents λ_k are constant. The complex constants c_k, $k = 1$ to N, depend on the initial conditions, i.e., on the particular value of the small perturbation applied. Note the similarity with the general expression of the perturbation of a *dc* solution in (2). Because the vectors $\overline{u}_k(t)$ are periodic, the extinction of the perturbation ($\lim_{t\to\infty} \Delta\overline{x}(t) = 0$) will only depend on the real part of the different exponents λ_k in (20). Due the periodicity of $\overline{u}_k(t)$, if any λ_k is increased in a multiple of the fundamental frequency $\lambda_k + jp\omega_o$, where p is an integer, perturbation $\Delta\overline{x}(t)$ will take the same value after any integer number of periods. Time tending to infinity implies an infinite number of periods, so the exponents λ_k are non-univocally defined. The problem is circumvented with the *Floquet multipliers*, which constitute a set of N numbers defining the stability properties of the periodic solution [1,5-7,31-35]. The Floquet multipliers m_k are related to the *Floquet exponents* λ_k through the expression:

$$m_k = e^{\lambda_k T} = e^{\lambda_k T + jp\omega_o T} \quad (21)$$

which resolves the non-univocity of λ_k. Whether the increment $\Delta\overline{x}(t)$ will decay to zero or grow unboundedly will solely depend on the limit value of m_k^n with n tending to infinity. Clearly, if any of the multipliers has a modulus bigger than one, the perturbation will tend to infinity and the solution will be unstable. The calculation of Floquet multipliers is cumbersome except in the case of very simple circuits. However, knowing the meaning of these multipliers and keeping in mind the non-univocal relationship (21) is essential to understand the stability properties of periodic solutions.

In most cases, the microwave designer makes use of the harmonic-balance method to obtain the steady-state periodic solution of the circuit analyzed, at the fundamental frequency

ω_o. Assuming for compactness a *piecewise* formulation (Fig. 7), the state variables will correspond to the harmonic components [10,20], going from *–NH* to *NH*, of the control voltages of the active devices, composing the unknown vector $\bar{V}_s$. This vector fulfills the following system of harmonic balance equations [5-6,20]:

$$\bar{H}(\bar{V}) = \bar{V}_s + \left[Z(jk\omega_o)\right]\bar{I}(\bar{V}_s) + \left[Z_G(jk\omega_o)\right]\bar{G} = 0 \qquad (22)$$

where the vector $\bar{G}$ contains the input generator signal(s) at the fundamental frequency ω_o and the linear matrices $\left[Z_I(jk\omega_o)\right]$, $\left[Z_G(jk\omega_o)\right]$ describe the passive network. Note that (22) is composed by a set of vector equations, at the different harmonic frequencies, which is indicated by the general dependence on $(jk\omega_o)$, where *k* goes from *–NH* to *NH*.

For the stability analysis of the steady-state solution $\bar{V}_s$, a small instantaneous perturbation is considered. The complex frequency s associated with this perturbation will give rise to a small increment $\Delta\bar{V}$ in the circuit variables at the mixing frequencies $jk\omega_o + s$. Due to the small amplitude of the perturbation, the nonlinear elements can be linearized about the periodic steady-state solution $\bar{V}_s$ [15,36-37]. This is conceptually similar to the linearization about the *dc* solution carried out under a small-signal stability analysis. However, the steady-state solution is now periodic and the linearization involves the calculation of the *conversion matrix* $\left.\frac{\partial\bar{I}}{\partial\bar{V}}\right|_s$, composed of the derivatives of the harmonic components of the nonlinear elements with respect to the harmonic components of the independent variables [36,37]. In the case, for instance, of the nonlinear transconductance current of a FET device, the conversion matrix will be composed of the derivatives of each harmonic of this current with respect to each harmonic of each of the two control voltages, the gate-to-source voltage and the drain-to-source voltage. On the other hand, due to the effect of the perturbation, the circuit reactive elements must be evaluated at the frequencies $jk\omega_o + s$. Because there are no generators at these frequencies, one obtains the following characteristic system:

$$\left\{ \left[U\right]+\left[Z(jk\omega_o+s)\right]\left.\frac{\partial \bar{I}}{\partial \bar{V}}\right|_s \right\} \Delta\bar{V}=\left[JH(jk\omega_o+s)\right]\Delta\bar{V}=0 \tag{23}$$

It is an homogeneous system, so in order to have $\Delta\bar{V}\neq 0$, the associated characteristic matrix $\left[JH(jk\omega_o+s)\right]$ must be singular. For stability, all the roots of the characteristic determinant $\det\left[JH(jk\omega_o+s)\right]=0$ must be located in the LHP. For *NH* tending to infinity, these roots agree with the Floquet exponents in (21) of the periodic solution, as shown in [31]. Due to the non-univocal relationship between Floquet exponents and multipliers (21), the poles will have the form $\sigma\pm j\omega+jp\omega_o$ or $\gamma+jp\omega_o$, with $-NH\le p\le NH$, with each set obtained for different *k* values being associated with the same Floquet multiplier and therefore providing the same information.

As an example, the characteristic determinant of a resonant circuit containing a nonlinear capacitance will be derived next (Fig. 15). The circuit is composed of a resistor, an inductance and a varactor diode [7,18]. As will be shown from certain input power, the circuit exhibits a *parametric instability*, leading to a frequency division by 2. When driven with sufficiently large input power, the varactor diode is able to exhibit negative resistance in a certain frequency interval about the small signal resonance frequency, which is due to a phase shift between current and voltage larger than 90º. In this example, the capacitance is modeled as $c(v)=a+bv$, with a = 1.0 pF, and b = 0.3 pF/V. The element values are R = 5 Ω, L = 10 nH and the input frequency is f_o = 3 GHz. For simplicity, the periodic steady-state solution is calculated considering only the fundamental frequency $\omega_o = 2\pi f_o$. The characteristic determinant is:

$$\det\left\{\left[U_3\right]+\left[Z(jk\omega_o+s)\right]\left[jk\omega_o+s\right]\left.\frac{\partial Q}{\partial V}\right|_s\right\}=$$

$$\det\left\{\left[U_3\right]+\begin{bmatrix}-j\omega_o+s & 0 & 0\\ 0 & s & 0\\ 0 & 0 & j\omega_o+s\end{bmatrix}\begin{bmatrix}R+L(-j\omega_o+s) & 0 & 0\\ 0 & R+Ls & 0\\ 0 & 0 & R+L(j\omega_o+s)\end{bmatrix}\begin{bmatrix}C_0 & C_{-1} & C_1\\ C_1 & C_0 & C_{-1}\\ C_2 & C_1 & C_0\end{bmatrix}\right\}=$$

$$=0 \tag{24}$$

where $[U_3]$ is the identity matrix of dimension $N = 3$. Note that C_i are the harmonic components of $c(v)$ evaluated at the steady state. The characteristic determinant in (24) has an order 8, which provides 8 generalized eigenvalues or poles. Equation (24) has been solved for three different values of the input voltage E_{in}. For each E_{in}, this involves two different steps (i) calculation of the nonlinear periodic regime, with diode voltage $v(t) = Ve^{j\omega_o t} + V^* e^{-j\omega_o t}$ and (ii) evaluation of the coefficients C_i, which are replaced into (24).

The dominant poles for the three different input voltages E_{in} are shown in Table III. For E_{in} = 1 V, there are two pairs of dominant poles, with the same real part, located about the divided-by-two frequency. They correspond to the mixing terms $\sigma \pm j\omega_a, \sigma \pm j(\omega_o - \omega_a)$ [remember (21)], and could have equally been written [5,24] as $\sigma \pm j(\omega_o / 2 - \Delta\omega)$, $\sigma \pm j(\omega_o / 2 + \Delta\omega)$. These two pairs of poles are on the LHP, so the solution at ω_o is stable. As E_{in} increases, the two pairs of poles approach each other, merge and split into two *independent* pairs of poles (with different σ values) at $\omega_o / 2$. For E_{in} = 2.525 V one of them is approximately located in the imaginary axis, which corresponds to a near *bifurcation* condition. The other pair is in the LHP. For E_{in} = 3 V, the critical pair of poles is in the RHP, which gives rise to transient to a divided-by-two regime.

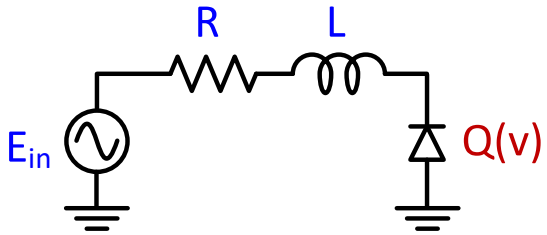

Fig. 15 Nonlinear resonator. the capacitance is modeled as $c(v) = a + bv$, with a = 1.0 pF, and b = 0.3 pF/V and the element values are R = 5 Ω, L = 10 nH.

Table II Dominant poles of the circuit in Fig. 15 for different E_{in}.

E_{in} (V)	$\sigma \pm j\omega/(2\pi)$
1	-2.5 10^9 ± j 1.419 10^9 -2.5 10^9 ± j 1.584 10^9
2.525	5.526 10^6 ± j 1.51 10^9
3	2.2944 10^8 ± j 1.51 10^9

In the general case, the direct calculation of the complex roots of $\det\left[JH(jk\omega_o + s)\right] = 0$ is nearly an impossible task. Instead, the Nyquist-stability criterion can be applied to this characteristic determinant. Replacing s by $j\omega$, the Nyquist plot is obtained calculating the function $\det\left[JH(jk\omega_o + j\omega)\right]$, where k goes from $-NH$ to NH. It is a complex function because only the "plus" sign is considered for the perturbation frequency ω. The Nyquist plot is obtained by sweeping ω and tracing $\mathrm{Im}\left\{\det\left[JH\right]\right\}$ versus $\mathrm{Re}\left\{\det\left[JH\right]\right\}$. Taking into account the aforementioned repetition of poles, the ω-sweep can be reduced to the interval $(0,\omega_o)$. Because the poles of the determinant function can only come from the linear matrices describing the passive networks, one can be sure that the number of clockwise encirclements N_T of the Nyquist plot will agree with the number of RHP zeroes of the determinant function, and therefore with the number of unstable eigenvalues. To obtain an accurate result, sufficient number NH of harmonic terms must be considered in the steady-state solution [15].

The Nyquist criterion has been applied to the R-L-diode circuit considered in Fig. 15. To obtain a valid result, two harmonic terms, ω_o and $2\omega_o$, had to be considered in the steady-state solution. The stability has been analyzed for three different values of the input amplitude E_{in} (Fig. 16). For $E_{in} = 1$ V, the circuit is stable since the plot (blue line) does not encircle the origin of the complex plane [see expanded view in Fig. 16(b)]. For $E_{in} = 3$ V, the circuit is unstable since the plot (red line) encircles the origin. For $E_{in} = 2.7$ V (solid line), the circuit is approximately at a bifurcation situation.

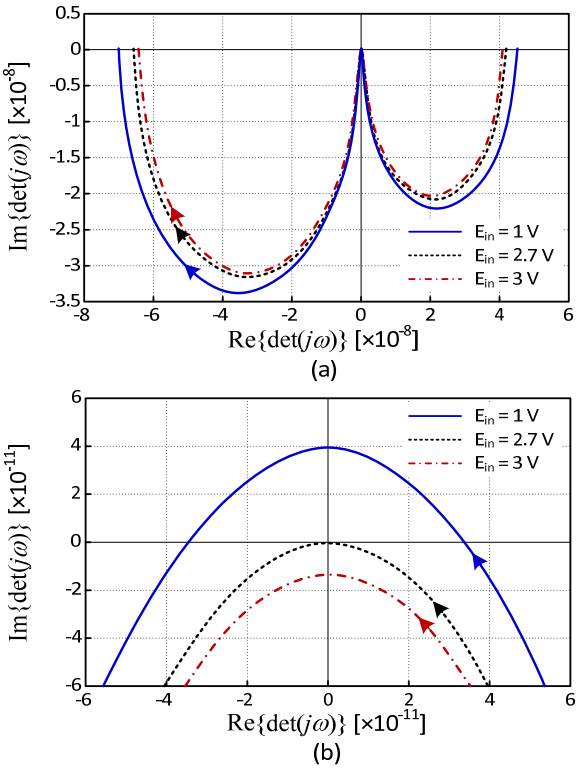

Fig. 16 Nyquist plots of the R-L-diode circuit in Fig. 15 for an input frequency is $f_o = 3$ GHz. (a) Three different values of input voltage are considered. (b) Expanded view.

The determinant function used to evaluate the circuit stability by means of a Nyquist plot can also be obtained through a recursive calculation of open loop transfer functions, by means of an extension of the so-called Normalized-Determinant Function, presented in [16]. The nonlinear dependences to be analyzed under open-loop conditions will be those susceptible to give rise to instability in large-signal conditions, that is, nonlinear transconductances and nonlinear capacitances [5]. From inspection of (23), this would imply a sequential replacement of each component $(k\omega_o + \omega)$ of each control voltage with an independent source $V_{m,k}^{ext}$ at the same frequency $(k\omega_o + \omega)$. For each *k* value, one should obtaining the increments undergone by the controlled current (or charge) at all the sidebands $p\omega_o + \omega$, with $-NH \le p \le NH$. This calculation must be recursively carried out for *k* going from *–NH* to *NH*. The steady-state solution must remain unaltered when doing so, so the circuit loops must remain closed at all frequencies $k\omega_o$ of the steady-state regime. Furthermore, at each open-loop calculation, the

input stimulus $V_{m,k}^{ext}$ must be zero at all sidebands different from $k\omega_o + \omega$. Thus, an ideal bandpass filter at $k\omega_o + \omega$ must be added to the external source stimulus, as demonstrated in [16].

Pole-zero identification

The characteristic matrix in (23) contains full information on the periodic signal response to small perturbations. Indeed, the exponents λ_k of (20) agree with the singularities of its associated determinant. When considering any small signal input at any sideband frequency $S_{in}(k\omega_o + s)$, the calculation of any possible output, at whatever the sideband frequency, $S_{out}(p\omega_o + s)$ will imply the inversion of a same characteristic matrix, agreeing with the one in (23). Thus, the denominator of any possible transfer function, agreeing with the characteristic determinant, should be the same, no matter the input or output considered in the particular transfer function [28-29]. The transfer function is formally the same when written in terms of the complex frequency *s* or in terms of $j\omega$, so this transfer function can be obtained introducing a small-signal input into the circuit, at the frequency ω, non-harmonically related to the fundamental frequency ω_o. Then, the harmonic-balance system is linearized about the periodic solution $\overline{V}_s$, with respect to a small-signal input at ω. As in the case of *dc* solutions, the small-signal input can be a current source I_n at the frequency ω. This source will be connected in parallel at a sensitive circuit node *n*, such as those corresponding to the transistor terminals. The circuit operates in a linear regime with respect to $I_n(\omega)$, so it can be analyzed by replacing the nonlinear elements with their conversion matrices. This will provide the following linearized system:

$$\left\{ \left[U\right] + \left[Z_I(jk\omega_o + j\omega)\right] \left.\frac{\partial \overline{I}}{\partial \overline{V}}\right|_s \right\} \Delta\overline{V} = -\left[Z_G(jk\omega_o + j\omega)\right] I_n \qquad (25)$$

The matrix on the left-hand side contains the full information on the circuit topology, so any closed-loop transfer function must share the same denominator. A convenient choice for the

output of the transfer function is the lower-frequency sideband $V_n(\omega)$ of the voltage at the node n at which the current generator $I_n(\omega)$ is connected [28-29]. Hence, the considered single input-single output transfer function is: $Z_{in}(\omega) = V_n(\omega) / I_n(\omega)$. The zeroes of the closed-loop transfer function will depend on the particular definition of this function, so undesired pole-zero cancellations may be obtained at particular locations of the current source. To extract the stability information from the transfer function $Z_{in}(\omega)$, this complex function is modeled with a quotient of polynomials in a manner similar to (19). As already known, the poles of a periodic solution at ω_o are also periodic, arranged in sets of the form $\gamma_m + jk\omega_o$ or $\sigma_m \pm j\omega_m + jk\omega_o$, where k is an integer number. Because of the periodicity of the poles, the frequency sweep in ω may be limited to $(0,\omega_o)$. Division into sub-intervals of smaller length, and using a lower order n, will generally increase the accuracy.

Pole-zero identification has been applied to the demonstrator power amplifier in Fig. 17, which operates at f_{in} = 1.5 GHz [24]. The circuit poles have been analyzed versus the input power P_{in} at the particular gate bias voltage V_{GS} = -1V [Fig. 18(a)]. To obtain the closed-loop transfer function, a small signal current source $I_d(\omega)$ has been connected to the drain node of one of the two transistors. The transfer function considered is $Z(\omega) = V_d(\omega) / I_d(\omega)$, which is calculated with the conversion-matrix approach. For each P_{in}, two analyses are carried out: (i) a harmonic balance analysis, to obtain the periodic large-signal steady state, and (ii) a conversion-matrix analysis, sweeping ω, to obtain the function $Z(\omega)$. Pole-zero identification is applied to each of the functions $Z(\omega)$ resulting versus P_{in}.

Transformations between poles of periodic solutions, taking into account (21), have been analyzed in depth in [5]. An example of these transformations is explained in the following. At small signal (P_{in} = -30 dBm), the amplifier in Fig. 17 exhibits two pairs of dominant complex-conjugate poles, associated with a same complex multiplier, located on the LHP. These two pairs of poles can be expressed as $\sigma \pm j(\omega_{in} / 2 \pm \Delta\omega)$. As P_{in} increases the two pairs of poles approach each other and merge ($\Delta\omega \to 0$) at P_{in} = 7 dBm. Since the dimension of the near-critical subspace must be preserved, after this merging they will split into two

independent pairs: $\sigma \pm j\omega_{in}/2, \sigma' \pm j\omega_{in}/2$. One of these two pairs crosses to the RHP at P_{in} = 8 dBm and to the LHP at P_{in} = 21 dBm. Within the interval (8 dBm, 21 dBm) the circuit exhibits a subharmonic oscillation at $\omega_{in}/2$. The results of pole-zero identification have been validated by obtaining the subharmonic steady-state solution in harmonic balance [Fig. 18(b)]. This analysis has required the use of an auxiliary generator [5] at the subharmonic frequency, to avoid undesired convergence to the coexistent non-divided solution. Details of this technique are given in the next paragraph. As gathered from the figure, the subharmonic solution arises when the pair of poles at $\omega_{in}/2$ crosses to the RHP and is extinguished when it crosses again to the LHP. The steady-state subharmonic component degenerates to zero amplitude at the two points at which the pair of poles at $\omega_{in}/2$ is exactly located in the imaginary axis. As shown in the next paragraph, this relevant property enables a straightforward detection of the boundaries of the stable interval.

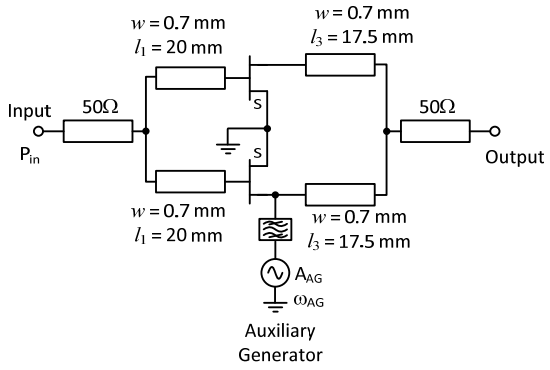

Fig. 17 Power amplifier demonstrator at f_{in} = 1.5 GHz.

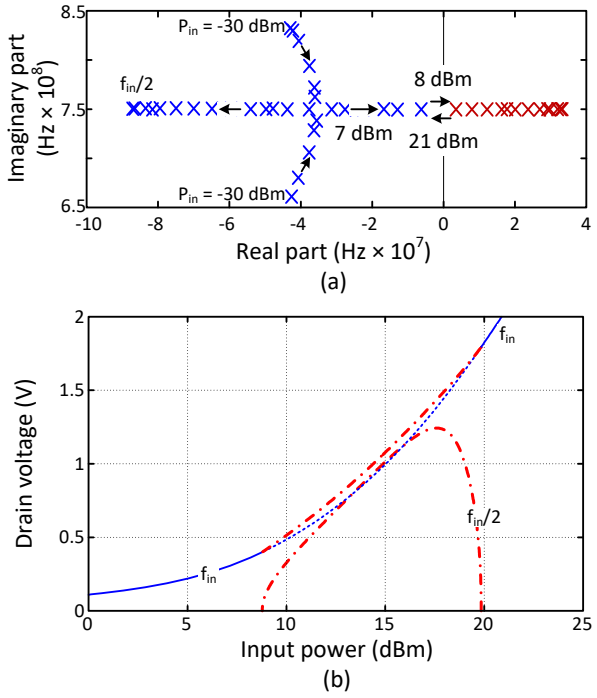

Fig. 18 Stability analysis of the circuit in Fig. 15 for V_{GS} = -1 V. (a) Pole-zero identification versus P_{in}. (a) Validation with harmonic balance, by tracing the solution curves at f_{in} and $f_{in}/2$ with the aid of an auxiliary generator [5,6]. The components of the subharmonic solution are represented in red.

Bifurcations

A bifurcation is a qualitative change in the stability of a steady-state solution or in the number of solutions when a parameter η is varied continuously [1-3,10]. The most relevant bifurcations in microwave circuit are those giving rise to oscillations and those giving rise to turning points, such as the points T_1 and T_2 in Fig. 3. The local bifurcations take place when either a real pole (for turning points) or a pair of complex conjugate poles cross the imaginary axis of the complex plane. The type of bifurcation depends on the original regime in which the circuit operates, *dc* or periodic, and the value of the critical frequency or frequencies, as shown in Table IV. A primary Hopf bifurcation is obtained when a pair of complex conjugate poles $\sigma \pm j\omega$ of a *dc* solution crosses the imaginary axis, which gives rise to the onset (or extinction) of an oscillation at the frequency of these poles. The secondary Hopf bifurcation takes place from a periodic regime at ω_o, and corresponds to the crossing of a pair of complex conjugate

poles $\sigma \pm j\omega$ through the imaginary axis, such that the frequency ω is non-harmonically related to ω_o. This gives rise to the onset (or extinction) of a self-oscillating mixer regime. The flip bifurcation also takes place from a periodic regime at ω_o, and corresponds to the crossing of a pair of complex conjugate poles $\sigma \pm j\omega_o/2$ through the imaginary axis, which gives rise to the onset (or extinction) of a subharmonic regime at $\omega_o/2$. Finally, the turning point bifurcation can occur in either dc or periodic regime and corresponds to the crossing of a real pole through the origin of the complex plane, which leads to a singularity of the steady-state equation system. This is often associated with hysteresis, as in Fig. 3, though in injection-locked oscillators it can also be associated with synchronization [5,6].

A relevant fact is that at the crossing point (bifurcation), the critical poles have zero real part. Therefore, bifurcation points can be obtained [10] replacing $s = j\omega$ in the expression for the characteristic determinant $\det(s) = 0$. To obtain the bifurcation point, the equation $\det(j\omega, \eta_b) = 0$, where η_b is the bifurcation parameter value, is solved in combination with the steady-state system. One will have $\omega = 0$, for a turning point, $\omega = \omega_a$, for a Hopf bifurcation and $\omega = \omega_o/2$, for a flip bifurcation. Because the frequency is real, the Hopf and flip bifurcation points fulfil conditions for a degenerate steady-state oscillation of amplitude tending to zero, at the respective frequencies ω_a and $\omega_o/2$ [5]. Taking this into account, an alternative technique to detect bifurcation points was proposed in [38]. The technique, based on the use of auxiliary generators, is compatible with commercial harmonic balance.

To detect Hopf and flip bifurcations, both leading to the onset of an oscillation, the aim will be to obtain the operation points at which this oscillation has amplitude tending to zero. An auxiliary generator (AG) is introduced into the circuit. The AG plays the role of the oscillation, so to obtain the bifurcation point its amplitude A_{AG} is set to very small value ($A_{AG} = \varepsilon$). The voltage (current) AG is connected in parallel (series) at a circuit node (branch). An ideal filter is necessary to prevent the short-circuiting or opening of frequency components different from ω_{AG}. In the case of a voltage generator, the ideal filter is connected in series with this generator

(see Fig. 17). The AG must fulfil the so-called non-perturbation condition [20], which ensures that it has no influence over the steady-state oscillation. For a voltage AG, the ratio between the AG current and the voltage delivered must be equal to zero, $Y_{AG} = I_{AG} / V_{AG} = 0$, at the operation frequency ω_{AG} .

In the case of a Hopf bifurcation [5-6], the additional unknowns enabling the fulfilment of $Y_{AG} = 0$ will be bifurcation parameter η and the frequency $\omega_{AG} = \omega_a$. Thus, one must solve $Y_{AG}(\eta_b, \omega_a) = 0$. In the case of a Hopf bifurcation arising from dc regime, this condition can be fulfilled through optimization in an AC analysis (due to the small amplitude of the AG). In the case of a Hopf bifurcation from periodic regime, condition $Y_{AG}(\eta_b, \omega_a) = 0$ will be an outer-tier equation and the pure harmonic-balance system will be the inner tier. The condition $Y_{AG}(\eta_b, \omega_a) = 0$ can also be solved through optimization, either with the conversion matrix approach (*large-signal small-signal* analysis) or with two-tone harmonic balance. In the case of a flip bifurcation [5.6], the AG will operate at the frequency $\omega_{AG} = \omega_o / 2$, and the additional unknowns will be η_b and the AG phase (or input source phase) ϕ_{AG}. The condition to be solved will be $Y_{AG}(\eta_b, \phi_{AG}) = 0$, with the pure harmonic balance system at the fundamental frequency $\omega_o / 2$ as inner tier.

Table IV Main types of bifurcation phenomena

Bifurcation	**Original regime**	**Critical poles** (poles crossing through the imaginary axis)	**Generated regime or phenomenon**
Primary Hopf	*dc*	$\sigma \pm j\omega$	Periodic oscillation at ω_o
Secondary Hopf	periodic at ω_o	$\sigma \pm j\omega$	Self-oscillating mixing regime ω_o and ω_a
Flip	periodic at ω_o	$\sigma \pm j\omega_o / 2$	Divided by 2 regime at $\omega_o / 2$
Turning point	*dc* or periodic	γ	Hysteresis (and synchronization in oscillators)

The bifurcation analysis enables a direct determination of the stability boundaries and, therefore, avoids the need for successive stability analyses, considering all the possible parameter values in an exhaustive manner. As an example, bifurcation analysis will be applied

to the demonstrator amplifier in Fig. 17. The parameters considered are the gate bias voltage V_{GS} and P_{in}. The bifurcation analysis in the plane defined by V_{GS} and P_{in} will provide a "map" from which we can predict what kind of operation (stable or unstable) the circuit will exhibit. This particular choice of parameters (V_{GS} and P_{in}) will also allow us to relate the small and large signal stability properties of the demonstrator amplifier.

A small signal stability analysis of this amplifier (under P_{in} = 0 W) shows that it should oscillate for bias voltage $-2.8\ V < V_{GS} < -1.2\ V$. This oscillation should be extinguished from certain input power P_{in} due to the natural reduction of negative resistance with the signal amplitude. To analyze this, the Hopf bifurcation locus will be calculated using an AG of voltage type (Fig. 17). The generator at the frequency $\omega_{AG} = \omega_a$, non-rationally related with ω_{in}, is connected to the drain terminal of one of the two transistors [24]. The AG amplitude is made arbitrarily small, solving the non-perturbation condition in terms of ω_a and the analysis parameters, that is: $Y_{AG}(V_{GS}, P_{in}, \omega_a) = 0$, with pure the HB system as an inner tier. This complex equation in three unknowns provides a curve in the plane V_{GS}, P_{in}. The locus has been represented in Fig. 19 with solid line. The locus is open on the right hand side. For all the Hopf locus points there is a pair of complex conjugate poles $\pm j\omega_a$ located in the imaginary axis. The frequency ω_a is expressible either as $\omega_a = \omega_{in}/2 - \Delta\omega$ or as $\omega_a = \omega_{in}/2 + \Delta\omega$ and varies through the locus, due to its autonomous nature. At the two edge points FH and FH', the frequency of the poles located in the imaginary axis tends to $\pm j\omega_{in}/2$. Because the dimension of the critical subspace must be preserved, at the two edge points there are two independent pairs of poles at the subharmonic frequency $\omega_{in}/2$ located in the imaginary axis.

In view of the above degeneration of the pole frequency to the subharmonic value $\pm j\omega_{in}/2$, there must be a flip bifurcation locus, completing the "map" in Fig. 19. In fact, two flip bifurcations had already been detected with the pole locus of Fig. 18, marked with "x" in Fig. 19. The flip bifurcation locus is traced with a small amplitude AG at the frequency $\omega_{AG} = \omega_{in}/2$, solving the complex equation $Y_{AG}(V_{GS}, P_{in}, \phi_{AG}) = 0$, which provides a curve in the

plane V_{GS}, P_{in}. The flip locus is closed and composed of two sections: a physical one (green) and an unphysical one (red). To understand this, one must take into account the following. At the two edge points of the Hopf locus there are two different pairs of poles at $\pm j\omega_{in}/2$. Through the flip locus, one of these two pairs stays on the imaginary axis $\pm j\omega_{in}/2$ and the other $\sigma \pm j\omega_{in}/2$ shifts from this axis either to the left $\sigma < 0$, in the green section of the flip locus, or the right ($\sigma > 0$), in the red section. When crossing the red section, the solution instability persists due to the presence of the pair of poles $\sigma \pm j\omega_{in}/2$, where $\sigma > 0$. The crossing of the green section does have a physical effect. The subharmonic component $\omega_{in}/2$ is either generated or extinguished when crossing the green section, this depending on the sense of variation of the parameter. All the above predictions have been validated with measurements, superimposed in Fig. 19. In these measurements, P_{in} has been increased in small steps, obtaining at each step the V_{GS} values that delimit the stable operation interval.

Fig. 20 compares the predictions of the bifurcation loci [Fig. 20(a)] with the results of pole-zero identification at constant P_{in} = 18 dBm, when increasing V_{GS}. In Fig. 20(b) the real part of the dominant poles has been traced versus P_{in}. A single value of real part is obtained when the dominant poles are complex conjugate at an incommensurable frequency $\sigma \pm j(\omega_{in}/2 \pm \Delta\omega)$. The merging of these poles ($\Delta\omega \to 0$) gives rise to two independent pairs of poles at the subharmonic frequency: $\sigma \pm j\omega_{in}/2$ and $\sigma' \pm j\omega_{in}/2$. Note that from the merging point, the real part of the poles splits into two different values.

For very low V_{GS}, the amplifier is stable, as expected. When increasing V_{GS}, the dominant pair of complex conjugate poles $\sigma \pm j\omega_a$ crosses the imaginary axis ($\sigma = 0$), which gives rise to the Hopf bifurcation H_1, well predicted by the Hopf locus in Fig. 20(a). From H_1, the amplifier periodic solution is unstable and it behaves instead in a self-oscillating mixer regime. At the Hopf bifurcation H_2, the complex conjugate poles $\sigma \pm j\omega_a$ cross again to the LHP and the amplifier periodic solution becomes stable. The incommensurable poles split into two pairs $\sigma \pm j\omega_{in}/2$ and $\sigma' \pm j\omega_{in}/2$ on the LHP and one of these pairs crosses the axis to

the RHP at the flip bifurcation F_1, giving rise to a frequency division by 2. The same pair of subharmonic poles crosses again to the LHP at the flip bifurcation F_2, from which the subharmonic regime is extinguished. The amplifier periodic solution becomes stable again at F_2.

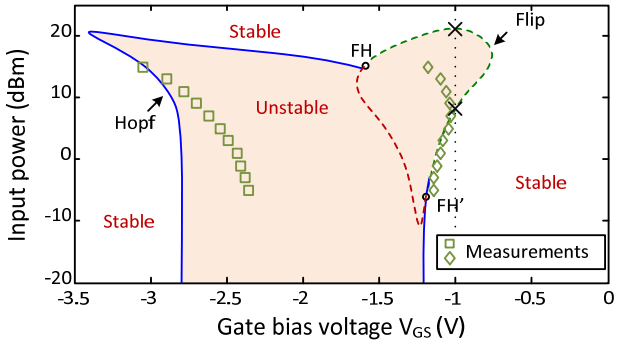

Fig. 19 Bifurcation loci (Hopf locus and flip locus) of the demonstrator in Fig. 17, with measurements superimposed. The unstable region is shadowed.

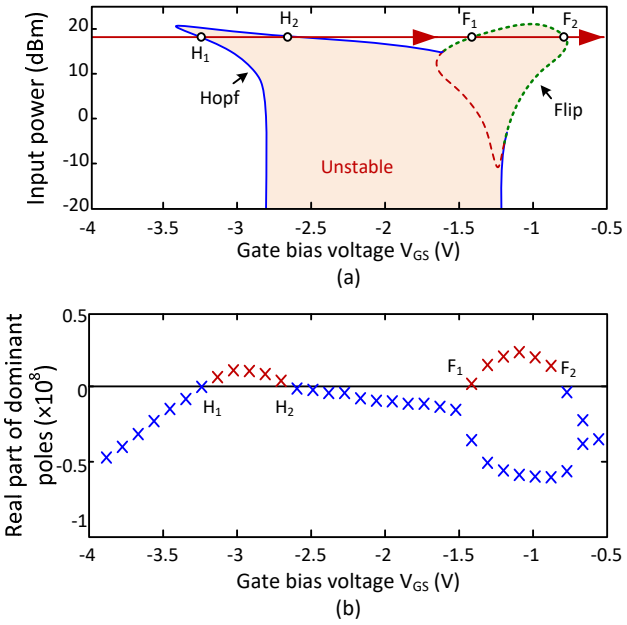

Fig. 20 Comparison between the predictions of the bifurcation loci (a) and pole-zero identification (b) at constant P_{in} = 18 dBm. The unstable region of (a) is shadowed.

Conclusions

Stability analysis methods have been presented in a self-contained manner. The main procedures have been described with analytical insight, enabling a comparison of their possible

limitations in terms of accuracy and complexity. Both small and large signal stability analysis has been considered and illustrated with examples that can be easily reproduced by the reader. The qualitative stability changes or bifurcations have also been addressed, with insight into their impact on the circuit behaviour.

References

[1] T.S. Parker, L.O. Chua, *Practical Numerical Algorithms for Chaotic Systems*, Springer-Verlag, New York, 1989.

[2] J. Guckenheimer and P. Holmes, *Nonlinear Oscillations, Dynamical Systems and Bifurcations of Vector Fields*. New York: Springer-Verlag, 1990.

[3] S. Wiggins, *Introduction to Applied Nonlinear Dynamical Systems and Chaos*. New York: Springer-Verlag, 1990.

[4] K. S. Kundert, "Introduction to RF simulation and its application," *IEEE J. Solid State Circuits,* vol. 34, no. 9, pp. 1298–1319, Sep., 1999.

[5] A. Suárez, *Analysis and Design of Autonomous Microwave Circuits. IEEE-Wiley*, Hoboken, (NJ) Jan. 2009.

[6] A. Suárez, R. Quéré, *Stability Analysis of Nonlinear Microwave Circuits. Artech House*, Norwood (Ma), Jan. 2003.

[7] A. Suárez, "Radiofrequency stability analysis", *Wiley Encyclopedia of Electrical and Electronics Engineering*, Oct. 2012.

[8] S. Jeon, A. Suárez, R. Rutledge, "Global stability analysis and stabilization of a Class-E/F amplifier with a distributed active transformer," *IEEE Transactions on Microwave Theory and Techniques*, vol. 53, no. 12, Dec. 2005, pp. 3712–3722.

[9] R. E. Collin, *Foundations for Microwave Engineering*, 2nd ed. Wiley Interscience, New York, 2001.

[10] V. Rizzoli and A. Neri, "State of the art and present trends in nonlinear microwave CAD techniques," *IEEE Trans. Microwave Theory Tech*., vol. 36, no. 2, pp. 343–356, Feb., 1988.

[11] *Advanced Design System*™ , Agilent Technologies.

[12] K. Ogata, *Modern Control Engineering.* Englewood Cliffs, NJ,: Prentice-Hall, 1980.

[13] G. Ioos, D. Joseph, *Elementary Stability and Bifurcation Theory*. New York. Springer, 1980.

[14] K. Kurokawa, "Some basic characteristics of broadband negative resistance oscillators," *The Bell System Technical Journal,* vol. 48, no. 6, pp. 1937-1955, Jul. –Aug. 1969.

[15] V. Rizzoli, A. Lipparini, "General stability analysis of periodic steady-state regimes in nonlinear microwave circuits," *IEEE Trans. on. Microwave Theory and Techniques*, vol. 33, no. 1, pp. 30 – 37, Jan. 1985.

[16] S. Mons, J.-C. Nallatamby, R. Queré, P. Savary, and J. Obregon, "A unified approach for the linear and nonlinear stability analysis of microwave circuits using commercially available tools," *IEEE Trans. Microwave Theory & Tech*., vol. 47, no. 12, pp. 2403–2409, Dec. 1999.

[17] S. Jeon, A. Suárez, R. Rutledge, "Analysis and elimination of hysteresis and noisy precursors in power amplifiers," *IEEE Transactions on Microwave Theory and Techniques,* vol. 54, no. 3, pp. 1096–1106, Mar. 2006.

[18] G. Sarafian, B. Z. Kaplan, "The dynamics of parametric frequency divider and some of its practical implications," *Electrical and Electronics Engineers in Israel, 1996., Nineteenth Convention of* , vol., no., pp. 523–526, 5-6 Nov. 1996.

[19] S. Basu, S. Maas, T. Itoh, "Stability analysis for large signal designo f a microwave frequency doubler", *IEEE Trans. Microwave Theory Tech.,* vol. 43, no. 12, pp. 2890–2898, Dec., 1995.

[20] R. Quéré, E. Ngoya, M. Camiade, A. Suarez, M. Hessane and J. Obregon, "Large signal design of broadband monolithic microwave frequency dividers and phase-locked oscillators," *IEEE Trans. on Microwave Theory and Techniques.,* vol. 41, no. 11, pp. 1928–1938, Nov., 1993.

[21] C. Barquinero, A. Suárez, A. Herrera, J. L. García, "Complete stability analysis of multifunction MMIC circuits," *IEEE Trans. on Microwave Theory and Techniques.,* vol. 55, no. 10, pp. 2024–2033, Oct., 2007.

[22] J. M. T. Thompson and H. B. Stewart, Nonlinear dynamics and chaos, Second Edition, Wiley, 2002.

[23] L. O. Chua, C. W. Wu, A. Huang, G-Q. Zhong, "A universal circuit for studying and generating chaos – Part I: routes to chaos", *IEEE Trans. on Circuits and Systems-I: Fundamental Theory and Applications,* vol. 40, no. 10, pp. 732–744, Oct., 1993.

[24] A. Suárez, F. Ramírez, “Detailed investigation of fundamental instability mechanisms in power amplifiers”, (invited) *Asia Pacific Microwave Conference*, Sendai (Japan), 2014.

[25] A. Platzker, W. Struble, "Rigorous determination of the stability of linear n-node circuits from network determinants and the appropriate role of the stability factor K of their reduced two-ports," in *Third International Workshop on Integrated Nonlinear Microwave and Millimeterwave Circuits,* pp. 93–107, 5–7, Oct. 1994.

[26] W. Struble, A. Platzker, “A rigorous yet simple method for determining stability of linear N-port networks [and MMIC application],” in 15th *Gallium Arsenide Integrated Circuit (GaAs IC) Symposium*, pp. 251 – 254, 1993.

[27] J. M. Rollett, "Stability and power-gain invariants of linear two ports," *Institute of Radio Engineers Transactions on Circuit Theory*, vol. CT-9, pp. 29–32, Mar. 1962.

[28] J. Jugo, J. Portilla, A. Anakabe, A. Suárez, and J. M. Collantes, "Closed-loop stability analysis of microwave amplifiers," *IEE Electronics Letters*, vol. 37, no. 4, pp. 226–228, Feb. 2001.

[29] A. Anakabe, J. M. Collantes, J. Portilla, et al. "Analysis and elimination of parametric oscillations in monolithic power amplifiers," *2002 IEEE MTT-S Int. Microwave Symp. Dig.*, Seattle, WA, Jun. 2002, pp. 2181–2184.

[30] N. Ayllon, J. M. Collantes, A. Anakabe, I. Lizarraga, S. Soubercaze-Pun, S. Forestier, “Systematic approach to the stabilization of multitransistor circuits”, *IEEE Trans. on Microwave Theory and Techniques*, vol. 59, no. 8, pp. 2073–2082, Aug. 2011.

[31] J. M. Collantes, I. Lizarraga, A. Anakabe, J. Jugo, “Stability verification of microwave circuits through Floquet multiplier analysis,” *2004 IEEE APCCAS*, Taiwan, 2004, pp. 997–1000.

[32] D. Woods, "Reappraisal of the unconditional stability criteria for active 2-port networks in terms of S parameters," *IEEE Trans. on Circuits and Systems,* vol.23, no. 2, pp. 73–81, Feb., 1976.

[33] R. W. Jackson, “Rollet proviso in the stability of linear microwave circuits – A tutorial.” *IEEE Trans. on. Microwave Theory and Techniques,* vol. 54, no. 3, March. 2006, pp. 993-1000.

[34] M. L. Edwards and J. H. Sinsky, "A new criterion for linear 2-port stability using geometrically derived parameters," *IEEE Trans on Microwave Theory and Techniques*, vol. 40, no. 12, pp. 2303–2311, Dec., 1992.

[35] F. Bonani and M. Gilli, "Analysis of stability and bifurcations of limit cycles in Chua's circuit through the harmonic-balance approach," *IEEE Transactions on Circuits and Systems-I,* vol. 46, no. 8, pp. 881–890, Aug., 1999.

[36] J. M. Paillot, J. C. Nallatamby, M. Hessane, R. Quéré, M. Prigent and J. Rousset, "A general program for steady state, stability, and FM noise analysis of microwave oscillators," *IEEE MTT Symposium,* 1990, pp. 1287–1290.

[37] V. Rizzoli, F. Mastri and D. Masotti, "General noise analysis of nonlinear microwave circuits by the piecewise harmonic balance technique," *IEEE Trans. on Microwave Theory and Techniques,* vol. 42, no. 5, pp. 807–819, May, 1994.

[38] A. Suarez, J. Morales, R. Quéré, "Synchronization analysis of autonomous microwave circuits using new global-stability analysis tools," *IEEE Trans. on Microwave Theory and Techniques*, vol. 46, no. 5, pp. 494–504, May 1998.